

OPTICAL PHOTOMETRY OF THE TYPE Ia SN 1999ee AND THE TYPE
Ib/c SN 1999ex IN IC 5179

Maximilian Stritzinger¹

Department of Physics, The University of Arizona, Tucson, AZ 85721

stritzin@as.arizona.edu

Mario Hamuy^{1,2}

*The Observatories of the Carnegie Institution of Washington, 813 Santa Barbara Street,
Pasadena, CA 91101*

mhamuy@ociw.edu

Nicholas B. Suntzeff

*National Optical Astronomy Observatories³, Cerro Tololo Inter-American Observatory, Casilla
603, La Serena, Chile*

nsuntzeff@noao.edu

R. C. Smith

*National Optical Astronomy Observatories³, Cerro Tololo Inter-American Observatory, Casilla
603, La Serena, Chile*

csmith@noao.edu

M. M. Phillips

Carnegie Institution of Washington, Las Campanas Observatory, Casilla 601, La Serena, Chile

mmp@lco.cl

José Maza

Departamento de Astronomía, Universidad de Chile, Casilla 36-D, Santiago, Chile

jose@das.uchile.cl

L. -G. Strolger

Department of Astronomy, University of Michigan, Ann Arbor, MI 48109-1090

loust@umich.edu

Roberto Antezana

Departamento de Astronomía, Universidad de Chile, Casilla 36-D, Santiago, Chile

`rantezan@das.uchile.cl`

Luis González

Departamento de Astronomía, Universidad de Chile, Casilla 36-D, Santiago, Chile

`lgonzale@das.uchile.cl`

Marina Wischnjewsky

Departamento de Astronomía, Universidad de Chile, Casilla 36-D, Santiago, Chile

`marina@das.uchile.cl`

Pablo Candia

National Optical Astronomy Observatories³, Cerro Tololo Inter-American Observatory, Casilla 603, La Serena, Chile

`candia@noao.edu`

Juan Espinoza

National Optical Astronomy Observatories³, Cerro Tololo Inter-American Observatory, Casilla 603, La Serena, Chile

David González

National Optical Astronomy Observatories³, Cerro Tololo Inter-American Observatory, Casilla 603, La Serena, Chile

Christopher Stubbs

Department of Astronomy, University of Washington, Box 351580, Seattle, WA 98195-1580

`stubbs@astro.washington.edu`

A. C. Becker⁴

Departments of Astronomy and Physics, University of Washington, Seattle, WA 98195

`becker@astro.washington.edu`

Eric P. Rubenstein

Department of Astronomy, Yale University, P.O. Box 208101, New Haven, CT 06520-8101

ericr@astro.yale.edu

Gaspar Galaz⁵

Carnegie Institution of Washington, Las Campanas Observatory, Casilla 601, La Serena, Chile

gaspar@azul.lco.cl

ABSTRACT

We present *UBVRIZ* lightcurves of the Type Ia SN 1999ee and the Type Ib/c SN 1999ex, both located in the galaxy IC 5179. SN 1999ee has an extremely well sampled lightcurve spanning from 10 days before B_{max} through 53 days after peak. Near maximum we find systematic differences ~ 0.05 mag in photometry measured with two different telescopes, even though the photometry is reduced to the same local standards around the supernova using the specific color terms for each instrumental system. We use models for our bandpasses and spectrophotometry of SN 1999ee to derive magnitude corrections (S-corrections) and remedy this problem. This exercise demonstrates the need of accurately characterizing the instrumental system before great photometric accuracies of Type Ia supernovae can be claimed. It also shows that this effect can have important astrophysical consequences since a small systematic shift of 0.02 mag in the $B - V$ color can introduce a 0.08 mag error in the extinction corrected peak B magnitudes of a supernova and thus lead to biased cosmological parameters. The data for the Type Ib/c SN 1999ex present us with the first ever observed shock breakout of a supernova of this class. These observations show that shock breakout occurred 18 days before B_{max} and support the idea that Type Ib/c supernovae are due to core collapse of massive stars rather than thermonuclear disruption of white dwarfs.

Subject headings: supernovae: Type Ia, Type Ib/c –optical photometry –SN 1999ee –SN 1999ex

¹Visiting Astronomer, Cerro Tololo Inter-American Observatory. CTIO is operated by AURA, Inc. under contract to the National Science Foundation.

²Hubble Fellow.

³Cerro Tololo Inter-American Observatory, Kitt Peak National Observatory, National Optical Astronomy Observatories, operated by the Association of Universities for Research in Astronomy, Inc., (AURA), under cooperative agreement with the National Science Foundation.

⁴Present address: Bell Laboratories, Lucent Technologies, 600 Mountain Avenue, Murray Hill, NJ 07974.

⁵Present address: Departamento de Astronomía y Astrofísica, P. Universidad Católica de Chile, Casilla 306, Santiago, Chile

1. Introduction

In recent years significant effort has gone into searching for and observing Type Ia supernovae (hereafter referred to as SNe) with the purpose of determining cosmological parameters. Despite this progress, most of SNe Ia observations have been limited to optical wavelengths, and relatively little is still known about the infrared (IR) properties of these objects. IR photometry of SNe has been limited to a handful of events, including the early work of Elias et al. (1981, 1985) and Frogel et al. (1987), and the most recent efforts by Jha et al. (1999), Hernandez et al. (2000), and Krisciunas et al. (2000). Combined IR studies of SNe Ia (Meikle 2000) have shown that SNe Ia display a scatter in peak absolute magnitude no larger than ± 0.15 mag in all three IR bands JHK , which is comparable to that obtained in the optical. To further exploit the usefulness of these objects as distance indicators, as well as to better understand the explosion mechanism and nature of SNe, more IR observations are clearly required.

Today the advent of new IR detectors enables us to obtain high quality observations and enlarge the hitherto small samples of SNe observed at these wavelengths. The “Supernova Optical and Infrared Survey” (SOIRS) was initiated in 1999 to make extensive IR and optical observations of bright candidates from the El Roble SN survey (Maza et al. 1981), and from the Nearby Galaxies Supernova Search (Strolger et al. 1999). Once objects were identified to be SN candidates, followup observations were conducted at several observatories including the Cerro Tololo Inter-American Observatory (CTIO) for optical/IR photometry, the Las Campanas Observatory (LCO) for IR photometry, and the European Southern Observatory (ESO) at Cerro Paranal and La Silla for optical/IR spectroscopy. During 1999-2000 this campaign resulted in a detailed study of 18 SNe. Of these events 10 were SNe Ia, 7 SNe II and 1 a Type Ib/c event.

This paper presents optical photometry for the two best-observed SNe in this survey, SN 1999ee and SN 1999ex. SN 1999ee was discovered by M. Wischnjewsky on a T-Max 400 film obtained by L. González on 1999 October 7.15 UT (JD 2,451,458.65) in the course of the El Roble survey (Maza et al. 1999). This SN exploded in IC 5179, a very active star-forming Sc galaxy with a heliocentric redshift of $3,498 \text{ km s}^{-1}$. Adopting a value for $H_0 = 63.3 \pm 3.5 \text{ km s}^{-1} \text{ Mpc}^{-1}$ (Phillips et al. 1999) along with a redshift of $3,239 \pm 300 \text{ km s}^{-1}$ in the Cosmic Microwave Background (CMB) Reference System, IC 5179 is located at a distance of $51.2 \pm 5.5 \text{ Mpc}$ ($\mu = 33.55 \pm 0.23$), which we adopt throughout this paper. An optical spectrum taken on 1999 October 9.10 revealed that SN 1999ee was a very young SN Ia, which led us to give it a high priority among our list of targets for followup observations.

In a rare occurrence IC 5179 produced a second SN within a few weeks from the discovery of SN 1999ee. The second SN (1999ex) was discovered on 1999 November 9.51 UT by Martin, Williams, & Woodings (1999) at Perth Observatory through the course of the PARG Automated Supernova Search. Initially we classified it as a Ic event (Hamuy & Phillips et al. 1999) based on the close resemblance to SN 1994I (Filippenko et al. 1995), although we now believe it belongs to an intermediate Ib/c class (Hamuy et al. 2002). Although SN 1999ex was discovered on 1999 November

9, examination of our data revealed that the object was present on our CCD images obtained 10 days before discovery. Further examination of the data showed that we had unintentionally detected the initial shock breakout resulting from the core bounce of SN 1999ex which, until now, has never been observed in a Ib/c event.

The observations gathered for SNe 1999ee and 1999ex have an unprecedented temporal and wavelength coverage and afford the opportunity to carry out a detailed comparison with explosion and atmosphere models. In this paper we report final reduced $UBVRIz$ lightcurves for both of these SNe. The photometry presented here is available in electronic form to other researchers.⁶ Section 2 discusses the observations and the data reduction process and Section 3 presents final results for both events. We proceed with a discussion in Section 4 after which we summarize our conclusions. Readers are to refer to K. Krisciunas et al. (2002, in preparation) and Hamuy et al. (2002), which include the analysis of IR photometry and optical/IR spectra, respectively.

2. Observations

Optical observations of IC 5179 began on 1999 October 8 and extended continuously through 1999 December 9, almost on a nightly basis. We collected the vast majority of data using the CTIO 0.91-m and YALO⁷ 1-m telescopes. On the 0.91-m telescope we used the standard 3×3 inch $UBV(RI)_{KC}$ Johnson/Kron-Cousins filter set and a Gunn z filter (Schneider, Gunn, & Hoessel 1983), in combination with a Tek 2048 \times 2046 CCD detector which provided a scale of 0.396 arcsec pix^{-1} . On the YALO telescope we used the dual-channel, optical-IR ANDICAM camera which was equipped with a Loral 2048 \times 2048 CCD (0.3 arcsec pix^{-1}), a Stromgren u filter and $BVRI$ filters. While the YALO BVI filters were close to the standard system, the u filter was narrower than the Johnson bandpass and the R filter was very wide compared to the standard bandpass. Figure 1 shows the filter bandpasses for both instruments compared to the standard ones defined by Bessell (1990) and Hamuy et al. (2001). We obtained a few additional photometric observations with the CTIO 1.5-m telescope as well as with the ESO NTT and Danish 1.54-m telescopes. Refer to Table 1 for the log of the observations, which includes the date of observation, telescope used, observatory, and observer name(s).

In order to reduce the effects due to atmospheric extinction we determined the brightness of each SN differentially with respect to a sequence of field stars in the region around IC 5179. Figure 2 shows a V band image identifying the photometric sequence. We obtained absolute photometry of these comparison stars with the CTIO 0.91-m telescope on 7 photometric nights in which we observed $UBVRI$ standards from the list of Landolt (1992) covering a wide range in brightness, color, and airmass. On four nights we also observed z band standards from the list of Hamuy et

⁶At <http://www.ociw.edu/~mhamuy/lightcurves.html>.

⁷YALO is a consortium consisting of Yale Univ., Univ. of Lisbon, Ohio State Univ., and NOAO.

al. (2001). In order to transform instrumental magnitudes to the standard Johnson/Kron-Cousins system we assumed linear transformations of the following form,

$$U = u - k_U X + CT_U(u - b) + ZP_U, \quad (1)$$

$$B = b - k_B X + CT_B(b - v) + ZP_B, \quad (2)$$

$$V = v - k_V X + CT_V(b - v) + ZP_V, \quad (3)$$

$$R = r - k_R X + CT_R(v - r) + ZP_R, \quad (4)$$

$$I = i - k_I X + CT_I(v - i) + ZP_I, \quad (5)$$

$$Z = z - k_z X + CT_z(v - z) + ZP_z, \quad (6)$$

where U, B, V, R, I, Z refer to magnitudes in the standard system, u, b, v, r, i, z refer to instrumental magnitudes measured with an aperture of 14 arcsec in diameter (the same employed by Landolt), k_i to the atmospheric extinction coefficient, X to airmass, CT_i to the color term, and ZP_i to the zero-point of the transformation. For each photometric night we used least-squares fits to solve for the photometric coefficients given above. Except for the U band the typical scatter in the transformation equations amounted to 0.01-0.02 mag (standard deviation), thus confirming the photometric quality of the night. For U the spread was typically 0.03-0.04 mag. Table 2 contains the $UBVRIz$ photometry of the sequence stars identified in Figure 2 along with the corresponding errors in the mean.

From the many different photometric nights of the SOIRS program we noticed that the color terms of the CTIO 0.91-m telescope varied little with time, thus allowing us to adopt average values. This offered the advantage of reducing the number of fitting parameters in equations 1-6 during the SN reductions. For the CTIO 1.5-m, NTT, and Danish 1.54-m telescopes we were also able to derive average color terms from observations of Landolt standards on multiple nights. For the YALO, on the other hand, we did not have observations of Landolt stars so we used the photometric sequence itself to solve for color terms. From the many nights of data we could not see significant changes in these coefficients, thus allowing us to adopt average values. Table 3 summarizes the average values for each telescope and associated filters. This table reveals that the color terms for the instrumental U and B bands are generally large owing to the rapid sensitivity drop of CCDs toward blue wavelengths, which effectively shifts the bandpasses to the red. Except for the YALO R filter the remaining color terms are close to zero, thus implying a good match of the instrumental bands to the standard system. The large color term for the YALO R filter is clearly not unexpected owing to its non-standard width (see Figure 1).

Before performing photometry of the SNe, we subtracted late time templates of the parent galaxy from all images in order to reduce light contamination using the method described by Filippenko et al. (1986) and Hamuy et al. (1994a). We obtained good-seeing moonless $UBVRIz$ images of IC 5179 with the CTIO 1.5-m telescope on 2001 July 16, nearly two years after discovery

of the SNe. We took three images of IC 5179 in $BVIz$ and two RU images with an exposure time of 300 seconds. We combined these to create deeper master images of the host galaxy for the subtraction process. The procedure used for galaxy subtraction consisted of four steps, each of which was performed with IRAF⁸ scripts. The steps included: (1) aligning the two images using field star positions (coordinate registration); (2) matching the point spread function (PSF) of the two images (PSF registration); (3) matching the flux scale of the two images (flux registration); (4) subtracting the galaxy image from the SN+galaxy image. To avoid subtracting the local photometric sequence from the subtracted image we restricted the subtraction to a small image section around the host galaxy. With this approach the local standards remained unaffected by the above procedure and we could proceed to carry out differential photometry for the SN and the local standards from the same image.

Upon completing galaxy subtraction we performed differential photometry for all images of the SNe using either aperture photometry (with the IRAF task PHOT) or PSF photometry (with the IRAF task DAOPHOT), depending on the SN brightness. When photon noise exceeded 0.015 mag (the uncertainty in an individual photometric measurement caused by non-Poissonian errors) for either SN, we used the more laborious PSF technique. The weather in Chile was very good around 1999 October/November and the seeing values at CTIO and ESO were always below 2.5 arcsec, and generally between 1-1.5 arcsec (FWHM). Hence, we chose an aperture of 2 arcsec to calculate instrumental magnitudes for the SNe and the comparison stars. Likewise, during PSF photometry we used a PSF fitting radius of 2 arcsec. While this aperture kept the sky noise reasonably low, it included a large fraction ($\sim 90\%$) of the total stellar flux, thus minimizing errors due to possible variations of the PSF across the image. For each frame we used the local standards to solve for the photometric transformation coefficients (equations 1-6). The advantage of doing differential photometry is that all stars in a frame are observed with the same airmass so that the magnitude extinction is nearly the same for all stars, thus reducing the number of free parameters in the transformation equations⁹. Moreover, having fixed the color terms to the average values, the photometric transformation for a single night only involved solving the zero point for each filter. Typically the scatter in the photometric transformation proved <0.02 mag (standard deviation).

⁸The Image Reduction and Analysis Facility (IRAF) is maintained and distributed by the Association of Universities for Research in Astronomy, under a cooperative agreement with the National Science Foundation.

⁹Note that we neglected here any color dependence of the extinction coefficient. In the B band where the second-order extinction is the highest – 0.02 mag per airmass per unit color – we could have made an error of 0.01 mag because of this assumption.

3. Results

3.1. SN 1999ee

Table 4 lists the resulting $UBVRIz$ photometry of SN 1999ee. The quoted errors correspond to uncertainties owing to photon statistics. We adopted a minimum error of 0.015 mag in an individual magnitude to account for uncertainties other than the Poissonian errors. This value is the typical scatter that we observe from multiple CCD observations of bright stars whose Poissonian errors are negligibly small. This table specifies whether we obtained the magnitudes via PSF fitting (DAO) or aperture photometry (PHOT). We made observations for a total of 50 nights.

Figure 3 presents the resulting lightcurves of SN 1999ee which reveal the exceptional sampling obtained. This figure also shows a systematic magnitude difference between the YALO and CTIO 0.91-m data in most bands. This is a well known problem in SN observations caused by the use of filters which do not exactly match each other (Suntzeff et al. 1988; Menzies 1989; Hamuy et al. 1990; Suntzeff 2000). Although the color terms derived for each filter have the specific purpose of allowing us to standardize instrumental magnitudes, these are obtained from stars with normal continuous spectra and are not expected to work perfectly with SNe which are characterized by strong absorption and emission spectral features. Figure 3 shows that the systematic differences varied with time as the SN evolved. They proved particularly pronounced in the U band due to the large departures of the instrumental filters from the Johnson bandpass. Near maximum light, the difference in the photometry was $\Delta(U, B, V, R, I) = (-0.14, -0.01, -0.04, +0.04, -0.03)$ in the sense YALO minus CTIO 0.91-m. One month later (JD 2,451,500) the difference was $(+0.17, +0.04, -0.05, +0.03, +0.04)$.

We attempted to fix this problem and compute magnitude corrections by convolving the spectrophotometry of SN 1999ee (Hamuy et al. 2002) with instrumental and standard bandpasses. Since we measured the SN magnitudes with photon detectors, a synthetic magnitude on the natural system must be calculated as the convolution of the object’s photon number distribution (N_λ) with the filter instrumental bandpass ($S(\lambda)$), i.e.,

$$mag = -2.5 \log_{10} \int N_\lambda S(\lambda) d\lambda + ZP, \quad (7)$$

where ZP is the zero-point for the magnitude scale. To a minimum $S(\lambda)$ should include the transparency of the Earth’s atmosphere, the filter transmission, and the detector quantum efficiency (QE). For the standard bandpasses we adopted the $UBVRI$ filter functions given by Bessell (1990) and the z function given by Hamuy et al. (2001). However, since the Bessell curves are meant for use with energy and not photon distributions (see Appendix in Bessell (1983)), it proved necessary to divide them by λ before employing them in equation 7 (Suntzeff et al. 1999; Hamuy et al. 2001). For the instrumental bandpasses we used transmission curves corresponding to the filters employed with the YALO and CTIO 0.91-m telescopes, nominal QE curves for the LORAL and Tek CCDs

used with both cameras, and an atmospheric transmission spectrum corresponding to one airmass. Note that we did not include here mirror aluminum reflectivities, the dichroic transmission for the YALO camera, and dewar window transmissions because we lacked such information.

To check if the resulting bandpasses provided a good model for those actually used at the telescopes we computed synthetic magnitudes for spectrophotometric standards (Hamuy et al. 1994b) and asked if the color terms derived from the synthetic magnitudes matched the observed values given in Table 3. We could only do this calculation for the $BVRIz$ filters since the spectrophotometric standards do not cover the entire U filter. We calculated synthetic color terms with equations 2-6, where b, v, r, i, z are the synthetic magnitudes for the YALO and CTIO 0.91-m instrumental bandpasses and B, V, R, I, Z are the synthetic magnitudes derived from the standard functions. Although we find an overall good agreement between the observed and synthetic color terms, small differences are present which suggest some differences between the nominal and the instrumental bandpasses used at the telescopes. Possible explanations for the differences are mirror reflectivities or any transmissivity of other optical elements of the instruments employed (e.g. the dichroic mirror used with YALO/ANDICAM). To solve this problem our approach consisted in applying wavelength shifts to our nominal instrumental bandpasses until we were able to reproduce exactly the measured color terms. The required shifts are summarized in Table 5. They are always less than 100 Å, except in the V and R YALO filters where they amount to 120 Å and 180 Å, respectively. Figure 1 displays the resulting functions.

Armed with the best possible models for our instrumental bands we used the spectrophotometry of SN 1999ee to compute magnitude corrections (S-corrections, hereafter) that should allow us to bring our observed photometry to the standard system. For the V filter the S-correction is

$$\Delta V = V - v - CT_V(b - v) - ZP_V, \quad (8)$$

where V is the SN synthetic magnitude computed with the Bessell function, and b, v are the SN synthetic magnitudes computed with the instrumental bandpasses. CT_V is the color term for the corresponding filter and ZP_V is a zero point that can be obtained from the spectrophotometric standards to better than 0.01 mag. Similar equations can be written for the other filters.

Figure 4 shows the S-corrections. For the CTIO 0.91-m system the corrections are generally small, which suggests that this instrument provides a good match to the standard system. The worst case occurs in the I band at late times where the shifts amount to 0.04 mag. The YALO instrument, on the other hand, is affected by large systematic shifts of 0.05 mag or more. The S-corrections are particularly large in the R filter, which is not unexpected considering the large departures from the standard band.

Figure 5 contains the $BVRIz$ lightcurves after applying S-corrections. A comparison with Figure 3 shows that the corrections help significantly in the V band at all epochs. In the B and I bands they only help at some epochs, while it is clear that we overcorrect in the R band at

all epochs. These differences are somewhat disappointing and are certainly due to an incomplete knowledge of the actual bandpasses employed at the telescopes. We explored if the problem could be due to a poor flux calibration of the SN spectra or to incorrect reddening corrections. For this purpose we applied a $\pm 0.1 E(B - V)$ artificial reddening to the SN spectra and re-computed the S-corrections. The result of this test is that the S-corrections change only by 0.005 mag in each direction, which implies that they are mostly determined by spectral features that vary on small wavelength scales compared to the bandpasses.

Although we do not feel we should use these S-corrections at this stage, this exercise demonstrates the need of accurately characterizing the instrumental system before great photometric accuracies of SNe Ia can be claimed. It also shows that this effect can have important astrophysical consequences since a small systematic shift of 0.02 mag in the $B - V$ color can introduce a 0.08 mag error in the extinction corrected peak B magnitudes of a SN and thus lead to biased cosmological parameters.

Returning to the uncorrected magnitudes of SN 1999ee, we used a high order Legendre polynomial to derive B_{max} of 14.93 ± 0.02 mag on JD 2,451,469.1 \pm 0.5, which indicated that the first observations began 10 days prior and the last observations were made 53 days after B_{max} . Likewise, we found V_{max} of 14.61 ± 0.03 mag about 2 days after B_{max} , in agreement with the template lightcurves derived by Leibundgut (1991). All filters covered the evolution of SN 1999ee extremely well through maximum light, past the secondary maximum through the onset of the exponential tail due to radioactive decay of $^{56}Co \rightarrow ^{56}Fe$. The z band lightcurve is the first of its type for a SN Ia event and reveals that the secondary maximum was only a few tenths of a magnitude fainter than the primary peak. Lightcurve parameters for all filters are given in Table 6. We estimated the uncertainties in the peak magnitudes from the scatter (peak to peak) in the photometric points around maximum in order to account for S-corrections.

We next performed lightcurve fits for this event using the templates derived by Hamuy et al. (1996). Figure 6 shows the BVI fits obtained with the 1991T and 1992bc templates that best matched the observed lightcurves. We stretched both templates by $(1+z)$ in order to account for time dilation, and modified them by K terms appropriate for the redshift of SN 1999ee (Hamuy et al. 1993). While the fits are reasonably good in the B and V bands, the templates do not provide a good match to the observed I lightcurve. The small decline rates of these templates ($\Delta m_{15}(B) = 0.87$ for SN 1992bc and 0.94 for SN 1991T) reveal that SN 1999ee was a slow-declining SN. In fact, a direct measurement of the decline rate gave $\Delta m_{15}(B) = 0.91 \pm 0.04$ which, after correction for host-galaxy extinction (Phillips et al. 1999) increased to 0.94 ± 0.06 mag (see section 4.1).

3.2. SN 1999ex

Table 7 contains the $UBVRIz$ photometry for SN 1999ex, as well as the method used to determine magnitudes. We present here a total of 32 nights of data. The lightcurves are presented

in Figure 7. Clearly the observations began well before maximum light thanks to our continuous followup of the host galaxy owing to the prior discovery of the Type Ia SN 1999ee. The first detection occurred on JD 2,451,481.6 (1999 October 30) in all filters. Excellent seeing images obtained on the previous night allowed us to place reliable upper limits to the SN brightness. Hence, in what follows we assume that shock breakout took place on JD 2,451,480.5. Given our nightly observations of IC 5179 we can attach an uncertainty of ± 0.5 day to this estimate. Undoubtedly, these are the earliest observations of a SN Ib/c, which reveal the SN evolution right after explosion. The most remarkable feature in this figure is the early dip in the U and B lightcurves – covering the first 4 days of evolution – after which the SN steadily rose to maximum light. The dip is absent in $VRIz$, yet it is possible to notice a slight change in the rate of brightening at the earliest epochs. This early upturn is reminiscent of the Type II SN 1987A (Hamuy et al. 1988) and the Type IIb SN 1993J (Schmidt et al. 1993; Richmond et al. 1994), both of which showed a first phase of rapid dimming followed by a second phase of steady brightening. Until now this dip had never been observed in a SN Ib/c. Although this is a generic feature of core collapse or thermonuclear explosion models, in Section 4.2 we argue that these observations favor the core collapse nature of SN Ib/c.

SN 1999ex reached $B_{max}=17.35\pm 0.02$ on JD 2,451,498.1 and $V_{max}=16.63\pm 0.04$ 3 days later on JD 2,451,501.2. This implies that our observations began 17 nights before B_{max} and extended until 24 days after peak. The upper limits on JD 2,451,480.5 strongly suggest that shock breakout occurred 18 days before B_{max} . Table 6 summarizes peak magnitudes and time of occurrence for each filter.

Figure 8 shows the $U - B$ and $B - V$ color curves for SN 1999ex, both of which track photospheric temperature variations. Initially the photosphere displayed a rapid cooling in which the $B - V$ color increased from 0.2 to 1.3 in only four days. Then the photospheric temperature increased so the SN evolved back to the blue. This phase extended for ten days through maximum light when SN 1999ex reached $B - V=0.6$. After reaching maximum light the SN again turned toward the red and the photosphere began to cool. The observations ceased 24 days past B_{max} . At that time there seemed to be an inflection of the $B - V$ curve toward the blue which probably coincided with the onset of the nebular phase when the SN went from being optically thick to optically thin.

4. Discussion

4.1. SN 1999ee

In order to obtain absolute magnitudes for SN 1999ee we first need to correct the apparent magnitudes for the effects of reddening caused by dust in both our Galaxy and the host galaxy. A small reddening of $E(B - V)_{Gal}=0.02$ can be attributed to our Galaxy in the direction of IC 5179 according to the IR dust maps of Schlegel, Finkbeiner, & Davis (1998). Interstellar absorption lines due to Na I D $\lambda\lambda 5890, 5896$, Ca II $\lambda 3934$, and Ca II $\lambda 3968$ at the redshift of IC 5179 could

be clearly seen in the spectra of SN 1999ee, with equivalent widths (EW) of 2.3, 0.8, and 0.6 Å, respectively (Hamuy et al. 2002). This suggests that a non-negligible amount of absorption in IC 5179 affected SN 1999ee. Calibrations between EW and reddening have been derived from high resolution spectra of Galactic stars (Richmond et al. 1994; Munari & Zwitter 1997), but these are only valid in the non-saturated regime ($EW(\text{Na I D}) < 0.8 \text{ \AA}$). Using SN data Barbon et al. (1990) derived the relation $E(B - V) \sim 0.25 \text{ EW}(\text{Na I D})$, which implies $E(B - V)_{\text{host}} = 0.58$ for SN 1999ee. We believe, however, that this value is of little usefulness owing to the uncertain dust to gas ratio around SNe (Hamuy et al. 2001).

Instead we can estimate the host galaxy’s reddening of SN 1999ee using the method described by Phillips et al. (1999) and Lira (1995). The de-reddening technique consists in comparing the observed colors of the SN to the intrinsic ones which are a function of the decline rate of the SN. $\Delta m_{15}(B)$ itself can be affected by the extinction due to the change of the effective wavelength of the B filter as the SN spectrum evolves (Phillips et al. 1999). From the direct measurement of $\Delta m_{15}(B)_{\text{obs}} = 0.91 \pm 0.04$ (after correction for time dilation and K-terms) and an internal reddening of $E(B - V)_{\text{host}} = 0.28 \pm 0.04$ (see below), we derive a true decline rate of $\Delta m_{15}(B) = 0.94 \pm 0.06$.

A direct comparison between the intrinsic colors $(B - V)_0$ and $(V - I)_0$ as predicted by Phillips et al. (1999) and the observed colors at maximum light (after correction for Galactic reddening, time dilation, and K-terms) yields $E(B - V)_{\text{max}} = 0.39 \pm 0.11$ and $E(V - I)_{\text{max}} = 0.29 \pm 0.11$. In addition using colors from the exponential tail we determine $E(B - V)_{\text{tail}} = 0.27 \pm 0.05$. Taking the weighted mean of $E(B - V)_{\text{max}}$, $E(B - V)_{\text{tail}}$, and $0.8E(V - I)_{\text{max}}$ we obtain the final estimation for host galaxy reddening $E(B - V)_{\text{host}} = 0.28 \pm 0.04$. Including Galactic extinction we get $E(B - V)_{\text{total}} = 0.30 \pm 0.04$ which, following Phillips et al. (1999), leads to the following monochromatic absorption values: $A_B = 1.24 \pm 0.17$, $A_V = 0.94 \pm 0.13$, and $A_I = 0.55 \pm 0.07$.

After applying these corrections to our BVI peak apparent magnitudes and using the distance modulus of 33.55 ± 0.23 based on the galaxy redshift, we obtain final absolute peak magnitudes of $M_B = -19.85 \pm 0.28$, $M_V = -19.87 \pm 0.26$, and $M_I = -19.43 \pm 0.24$. For its decline rate of $\Delta m_{15}(B) = 0.94 \pm 0.06$, SN 1999ee fits well with the peak luminosity-decline rate relation derived by Phillips et al. (1999).

Instead of adopting a distance to solve for absolute magnitudes, we can now solve for the distance to IC 5179 using the absolute magnitudes of SNe Ia recently calibrated with Cepheids. Note that we are not using the previous redshift based absolute magnitudes so that this is an independent test. The Cepheid-based absolute magnitudes (corrected for reddening and normalized to a $\Delta m_{15}(B) = 1.10$) of the SNe Ia calibrators used in Phillips et al. (1999) are $M_B = -19.61 \pm 0.09$, $M_V = -19.58 \pm 0.08$, and $M_I = -19.29 \pm 0.10$. For $\Delta m_{15}(B) = 0.94 \pm 0.06$, the luminosity-decline rate relation mentioned above predicts absolute magnitudes of $M_B = -19.72 \pm 0.12$, $M_V = -19.67 \pm 0.11$, and $M_I = -19.34 \pm 0.12$ for SN 1999ee. From the peak apparent magnitudes we obtain distance moduli of $\mu_B = 33.42 \pm 0.21$, $\mu_V = 33.35 \pm 0.17$, and $\mu_I = 33.46 \pm 0.14$ hence yielding $\mu_{\text{avg}} = 33.42 \pm 0.10$ for IC 5179. This value compares well with $\mu = 33.55 \pm 0.23$ derived from the galaxy redshift.

Figure 9 shows the $(B - V)_0$ and $(V - I)_0$ color curves of SN 1999ee corrected for $E(B - V)_{total}=0.30$, compared to the template curves of the slow-declining SNe 1992bc (solid line) and SN 1991T (dotted line), both adjusted to match the colors of SN 1999ee at maximum light, time dilated, and K-corrected. This comparison reveals that, although SN 1999ee had the typical trends displayed by other SNe Ia, it is not possible to fit its color at all epochs with a single reddening correction. SN 1992bc seems to provide a better match in $V - I$ before day +30 but after that epoch there is clear mismatch. SN 1991T, on the other hand, provides a good fit in $B - V$ yet a poor match in $V - I$. This demonstrates that SNe Ia with nearly the same decline rate do not have identical color curves. These examples raise doubts about the derivation of reddening from the shapes of the color curves, as advocated by Riess, Press, & Kirshner (1996). The method implemented by Phillips et al. (1999), instead, does not use information on the shape of the color curve but only the color at individual epochs.

4.2. SN 1999ex

SN 1999ex also showed clear absorption features due to interstellar lines of Na I D $\lambda\lambda 5890, 5896$, Ca II $\lambda 3934$, and Ca II $\lambda 3968$ at the redshift of IC 5179. The equivalent widths of 2.8, 1.8, and 0.9 Å measured for these lines (Hamuy et al. 2002) suggest even more dust absorption than for SN 1999ee. As mentioned above, however, it proves difficult to derive dust absorption from interstellar lines owing to the very uncertain dust to gas ratio around SNe. A lower limit to the peak absolute magnitudes of SN 1999ex can be derived assuming $E(B - V)_{Gal}=0.02$ (Schlegel, Finkbeiner, & Davis 1998). Omitting K-corrections (which are expected to be <0.02 mag, assuming the K-terms for SNe Ib/c are similar for SNe Ia), we get $M_B < -16.28 \pm 0.23$, $M_V < -16.98 \pm 0.23$, and $M_I < -17.61 \pm 0.23$ for SN 1999ex. Assuming that the amount of reddening affecting SN 1999ex is not radically different than $E(B - V)_{host}=0.28 \pm 0.04$ derived from SN 1999ee we get absolute magnitudes which may be considered representative of what the actual reddening might give. With this assumption we obtain $M_B = -17.44 \pm 0.28$, $M_V = -17.86 \pm 0.26$, and $M_I = -18.12 \pm 0.24$. These calculations illustrate how including host galaxy reddening affect the absolute magnitudes and, perhaps more importantly, the bolometric lightcurve (see below).

Although the initial dip and UV excess observed in SN 1999ex had never been observed before among Ib/c events, it was also observed in the Type II SN 1987A (Hamuy et al. 1988) and the Type IIb SN 1993J (Schmidt et al. 1993; Richmond et al. 1994). For these SNe II it is thought that the initial dip corresponded to a phase of adiabatic cooling that ensued the initial UV flash caused by shock emergence which super-heated and accelerated the photosphere. The following brightening is attributed to the energy deposited behind the photosphere by the radioactive decay of $^{56}Ni \rightarrow ^{56}Co$ and $^{56}Co \rightarrow ^{56}Fe$. Although the lightcurve of SN 1999ex bears qualitative resemblance to SN 1987A and SN 1993J, in those cases the initial peaks were relatively brighter and the dips in the lightcurves occurred ~ 8 days after explosion compared to 4 days in SN 1999ex. This suggests that SN 1999ex also was a core collapse SN and that the photometric differences could be due to the hydrogen that

the progenitors of SN 1987A and SN 1993J were able to retain. Woosley et al. (1987) computed Type Ib SN models consisting of the explosion of a $6.2 M_{\odot}$ helium core. Their Figure 7 shows the bolometric luminosities of three models with different explosion energies and ^{56}Ni nucleosynthesis. Despite the different lightcurve shapes and peak luminosities, all three models show an initial peak followed by a dip a few days later and the subsequent brightening caused by $^{56}\text{Ni} \rightarrow ^{56}\text{Co} \rightarrow ^{56}\text{Fe}$, making them good models for SN 1999ex.

We proceed now to compute a bolometric lightcurve for SN 1999ex in order to carry out a comparison with the models. A first approach consists in performing a blackbody (BB) fit at each epoch and derive analytically the total flux from the corresponding Planck function. Our fitting procedure consists in computing synthetic magnitudes in the Vega system (Hamuy et al. 2001) for BB curves reddened by $E(B - V)_{Gal}=0.02$ and $E(B - V)_{host}=0.28$, performing a least-squares fit to the SN BVI magnitudes, and deriving the color temperature and angular radius that yield the best match to the observed photometry. Figure 10 illustrates the fits for eight representative epochs. Note that, while the BB curve provides excellent fits during the first days of SN evolution, by day 4 since explosion the observed U flux begins to fall below the BB curve. This is a result of the strong line blanketing at these wavelengths, assuming the opacities for SNe Ib/c are similar to SNe Ia (Pinto & Eastman 2000). Note also that, although the R and z magnitudes are not included in the fits, they match well the BB curves derived from the BVI photometry. Table 8 summarizes the parameters yielded by the BB fits for all epochs. Figure 11 shows that the photospheric angular radius showed a steady increase which reflects the expansion of the SN ejecta. During the first 4 days the photospheric temperature dropped due to the adiabatic cooling that followed shock breakout, after which the temperature increased due to radioactive heating and then dropped again owing to expansion. Note that, as expected, this curve bears close resemblance to the color curves shown in Figure 8. The resulting bolometric lightcurve is plotted in the top panel of Figure 12 (closed circles) and the corresponding values can be found in Table 8. For comparison the bottom panel shows the curve obtained by assuming $E(B - V)_{host}=0.00$.

An alternative route to derive bolometric fluxes is to perform a direct integration of the SN $UBVRIZ$ broad-band magnitudes. For this purpose we use the $UBVRIZ$ magnitudes of Vega (Hamuy et al. 1992, 2001) and its spectral energy distribution (Hayes 1985) to derive conversion factors between broad-band magnitudes and monochromatic fluxes for the standard photometric system shown in Figure 1. With these assumptions a zero magnitude star has monochromatic fluxes of $(3.98, 6.43, 3.67, 2.23, 1.17, 0.82) \times 10^{-9}$ ergs $\text{sec}^{-1} \text{cm}^{-2} \text{\AA}^{-1}$ for U, B, V, R, I, z , which have equivalent wavelengths of 3570, 4413, 5512, 6585, 8068, and 9058 \AA , respectively. The resulting $U - z$ bolometric fluxes are listed in Table 8 and shown with open circles in Figure 12, both for $E(B - V)_{host}=0.28$ (top) and $E(B - V)_{host}=0.00$ (bottom). Since the SN emitted more flux beyond the $U - z$ wavelength range, this approach is expected to give a lower limit to the actual luminosity. Not surprisingly, the resulting fluxes lie well below the BB fluxes. The BB fits to the BVI magnitudes may also underestimate the true flux by a few dex owing to line blanketing in the B band. On the other hand, flux redistribution of the missing B flux could show up in the VI

bands and compensate for this flux deficit. Without a detailed atmosphere model for SNe Ib/c it proves difficult to quantify the difference between the BB and the true SN luminosity. In the case of SN 1987A – the SN with the best wavelength coverage – the *BVI* BB fit yields a flux ~ 0.05 dex greater than the $U \rightarrow M$ bolometric flux of Suntzeff & Bouchet (1990), throughout the optically thick phase of the SN. We believe therefore that the BB fits to SN 1999ex are probably within 0.1 dex from the true bolometric luminosity.

Figure 12 (top) reveals that the major difference between the BB and the $U - z$ curves is that the initial dip is not present in the $U - z$ integration. This is due to the fact that the SN photosphere was initially hot so that a significant fraction of the total flux was emitted at wavelengths shorter than 3500 Å. The BB fit on the other hand, provides such an excellent fit to the $U - z$ magnitudes at these epochs (Figure 10) that it must provide a better approximation to the true flux. Figure 12 (bottom) also reveals that the initial dip is less obvious in the BB curve when we assume $E(B - V)_{host} = 0.00$. Although this hypothesis is very unlikely given the strong interstellar absorption lines in the spectrum of SN 1999ex, this is illustrative of the effect reddening has on the bolometric lightcurve of SN 1999ex, which will in turn affect future calculations of the progenitor system.

Among the three SN Ib models of Woosley et al. (1987) model 6C – characterized by a kinetic energy of 2.73×10^{51} ergs and $0.16 M_{\odot}$ of ^{56}Ni – provides the best match to the BB lightcurve of SN 1999ex (Figure 12, top panel). The agreement is remarkable considering that we are not attempting to adjust the parameters. The initial peak and subsequent dip have approximately the right luminosities although the evolution of SN 1999ex was somewhat faster. The following rise and post-maximum evolution is well described by the model.

The observation of the tail of the shock wave breakout in SN 1999ex and the initial dip in the lightcurve provides us with an insight on the type of progenitor system for SNe Ib/c. Several different models have been proposed as progenitors for this type of SNe. One possibility is an accreting white dwarf which may explode via thermal detonation upon reaching the Chandrasekhar mass (Sramek, Panagia, & Weiler 1984; Branch & Nomoto 1986). These models are expected to produce lightcurves with an initial peak that corresponds to the emergence of the burning front, a fast luminosity drop due to adiabatic expansion, and a subsequent rise caused by radioactive heating. Given the compact nature of the progenitor ($\sim 1,800$ km) the cooling time scale by adiabatic expansion is only a few minutes (P. Höflich 2002, private communication) and the lightcurve is entirely governed by radioactive heating (Höflich & Khokhlov 1996). Hence, these models are not expected to show an early dip at a few days past explosion as is observed in SN 1999ex. The second and more favored model for SNe Ib/c consists of core collapse of massive stars ($M_{ZAMS} > 8 M_{\odot}$) which lose their outer H envelope before explosion. Within the core collapse models, there are two basic types of progenitor systems: 1) a massive ($M_{ZAMS} > 35 M_{\odot}$) star which undergoes strong stellar winds and becomes a Wolf-Rayet star at the time of explosion (Woosley, Langer & Weaver 1993), and 2) an exchanging binary system (Shigeyama et al. 1990; Nomoto et al. 1994; Iwamoto et al. 1994) for less massive stars. The resulting SNe have bolometric lightcurves containing an

initial shock breakout followed by a dip. Since the initial radii of these progenitors are ~ 100 times greater than that of white dwarfs, the dip occurs several days after explosion (Woosley et al. 1987; Shigeeyama et al. 1990; Woosley, Langer & Weaver 1993, 1995), very much like SN 1999ex.

Although a detailed modeling of SN 1999ex is beyond the scope of this paper, the fact that we were able to observe the initial shock break out followed by a dip within four days since explosion lends support to the idea that SNe Ib/c are due to the core collapse of massive progenitors rather than the thermonuclear disruption of white dwarfs. This is a prediction that could not have been decisively made prior to these observations.

In Figure 13 we present a comparison of the B and V band lightcurves of SN 1999ex with SN 1994I (Richmond et al. 1996) which proved spectroscopically similar to SN 1999ex (Hamuy et al. 2002) and the Type Ic SN 1983V (Clocchiatti et al. 1997). Despite their photospheric similarities, Figure 13 clearly shows that SN 1999ex had a much broader peak compared to SN 1994I. In addition we see that after reaching maximum light SN 1994I had a more rapid decline rate than SN 1999ex. These differences most likely indicate that SN 1999ex was able to retain more of an envelope prior to core collapse thus, increasing the diffusion time for the energy produced from the radioactive decay of ^{56}Ni to ^{56}Co (Arnett 1996). SN 1983V on the other hand has very limited sampling of data, however the width of its lightcurve and subsequent tail are similar to SN 1999ex indicating a more similar type of progenitor.

Figure 14 displays the $B - V$ color curves of SN 1999ex, SN 1994I, and SN 1983V. From B_{max} all three SNe evolved rapidly towards the red until approximately 15 to 20 days later in which they turned back towards the blue when the SNe became optically thin. It is not possible to compare the color evolution at earlier epochs since SN 1999ex is the only object with data at this early time.

4.3. Color evolution of Ia and Ib/c events

In the next years there will be several surveys of high- z SNe, with the main purpose of deriving cosmological parameters from SNe Ia. Given the large number of potential SNe to be discovered and the dim apparent magnitudes of the high- z objects, it will prove difficult to obtain a classification spectrum for all of the SN candidates. Hence, it will prove important to figure out photometric means to separate different types of SNe. The lightcurves themselves will be valuable tools at separating SNe II with plateau like evolutions from the Ia's that display a bell-shaped lightcurve. However, SNe Ib/c and SNe Ia have similar lightcurve shapes making hard to distinguish both types. As shown in Figure 15 the $B - V$ color curves of the Type Ia SN 1999ee and the Type Ib/c SN 1999ex reveal very different behaviors, especially before maximum light. But the post-maximum $B - V$ evolution of SN 1999ex is not so radically different than that of a fast-declining SNe Ia. However, with early-time photometry, colors offer a potentially useful method to help discriminate between these two types of SNe.

5. Conclusions

In a rare occurrence two SNe were observed simultaneously in IC 5179 at a redshift of $z = 0.01$ between 1999 October-December. For each image of these SNe we performed galaxy subtraction of late time images of their host galaxy after which we extracted $UBVRIZ$ magnitudes. We obtained well-sampled lightcurves including the first z band observations for a SN Ia and SN Ib/c.

Observations of the Type Ia SN 1999ee span from 10 days prior to B_{max} to 53 days afterwards. SN 1999ee was characterized by a slow decline rate of $\Delta m_{15}(B) = 0.94 \pm 0.06$. We estimate a value of host-galaxy reddening of 0.28 ± 0.04 which we use to derive reddening-free peak absolute magnitudes of $M_B = -19.85 \pm 0.28$, $M_V = -19.87 \pm 0.26$, and $M_I = -19.43 \pm 0.24$. SN 1999ee is among the most luminous SNe Ia and fits well in the peak luminosity-decline rate relation for SNe Ia.

Near maximum we find systematic differences ~ 0.05 mag in photometry measured with two different telescopes, even though the photometry is reduced to the same local standards around the supernova using the specific color terms for each instrumental system. We use models for our bandpasses and spectrophotometry of SN 1999ee to derive magnitude corrections (S-corrections) and remedy this problem. This exercise demonstrates the need of accurately characterizing the instrumental system before great photometric accuracies of Type Ia supernovae can be claimed. It also shows that this effect can have important astrophysical consequences since a small systematic shift of 0.02 mag in the $B - V$ color can introduce a 0.08 mag error in the extinction corrected peak B magnitudes of a supernova and thus lead to biased cosmological parameters.

The data for the second SN observed in this galaxy – Type Ib/c SN 1999ex – present us with the first ever observed shock breakout of a supernova of this class. These observations show that shock breakout occurred 18 days before B_{max} and support the idea that Type Ib/c supernovae are due to core collapse of massive stars rather than thermonuclear disruption of white dwarfs. The comparison of the lightcurves of SN 1999ex to other SNe Ic events like SN 1983V and SN 1994I reveals large photometric differences among this class of objects, probably due to variations in the properties of the envelopes of their progenitors and/or explosion energies. Future theoretical modeling of this event along with spectral analysis and construction of a bolometric lightcurve will provide insight on relevant parameters describing its progenitor.

M.S. is very grateful to Cerro Tololo for allocating an office and providing computer facilities while in La Serena (where the first draft of this paper was prepared) as well as to Mark Wagner for providing computer facilities in Tucson. We are very grateful to the YALO team for their service observing observations for this program and to the CTIO and ESO visitor support staffs for their assistance in the course of our observing runs. M.S. acknowledges support by the Hubble Space Telescope grant HST GO-07505.02-96A. M.H. acknowledges support provided by NASA through Hubble Fellowship grant HST-HF-01139.01-A awarded by the Space Telescope Science Institute, which is operated by the Association of Universities for Research in Astronomy, Inc., for NASA, under contract NAS 5-26555. This research has made use of the NASA/IPAC Extragalactic Database

(NED), which is operated by the Jet Propulsion Laboratory, California Institute of Technology, under contract with the National Aeronautics and Space Administration. This research has made use of the SIMBAD database, operated at CDS, Strasbourg, France.

REFERENCES

- Arnett, W. D. 1996, *Supernovae and Nucleosynthesis* (Princeton:Princeton Univ. Press)
- Barbon, R., Benetti, S., Capellaro, E., Rosino, L., & Turatto, M. 1990, *A&A*, 237, 79
- Bessell, M. S. 1983, *PASP*, 95, 480
- Bessell, M. S. 1990, *PASP*, 102, 1181
- Branch, D., & Nomoto, K. 1986, *A&A*, 164, L13
- Clocchiatti, A., et al. 1997, *ApJ*, 483, 675
- Elias, J. H., Frogel, J. A., Hackwell, J. A., & Persson, S. E. 1981, *ApJ*, 251, L13
- Elias, J. H., Matthews, K., Neugebauer, G., & Persson, S. E. 1985, *ApJ*, 296, 379
- Filippenko, A. V., Porter, A. C., Sargent, W. L. W., & Schneider, D. P. 1986, *AJ*, 92, 1341
- Filippenko, A. V., et al. 1995, *ApJ*, 450, L11
- Frogel, J. A., Gregory, B., Kawara, K., Laney, D., Phillips, M. M., Terndrup, D., Vrba, F., & Whitford, A. E. 1987, *ApJ*, 315, L129
- Hamuy, M., Suntzeff, N. B., González, R., & Martin, G. 1988, *AJ*, 95, 63
- Hamuy, M., Suntzeff, N. B., Bravo, J., & Phillips, M. M. 1990, *PASP*, 102, 888
- Hamuy, M., Walker, A. R., Suntzeff, N. B., Gigoux, P., Heathcote, S. R., & Phillips, M. M. 1992, *PASP*, 104, 533
- Hamuy, M., Phillips, M. M., Wells, L. A., & Maza, J. 1993, *PASP*, 105, 787
- Hamuy, M., et al. 1994a, *AJ*, 108, 2226
- Hamuy, M., Suntzeff, N. B., Heathcote, S. R., Walker, A. R., Gigoux, P., & Phillips, M. M. 1994b, *PASP*, 106, 566
- Hamuy, M., Phillips, M. M., Suntzeff, N. B., Schommer, R. A., Maza, J., Smith, R. C., Lira, P., & Avilés, R. 1996, *AJ*, 112, 2438
- Hamuy, M., & Phillips, M. M. 1999, *IAU Circ.* 7310

- Hamuy, M., et al. 2001, *ApJ*, 558, 615
- Hamuy, M., et al. 2002, *AJ*, 124, 417
- Hayes, D. S. 1985, in *Calibration of Fundamental Stellar Quantities*, ed. D. S. Hayes, L. E. Pasinetti, & A. G. Philip (Dordrecht: Reidel), 225
- Hernandez, M., et al. 2000, *MNRAS*, 319, 223
- Höflich, P., & Khokhlov, A. 1996, *ApJ*, 457, 500
- Iwamoto, K., Nomoto, K., Höflich, P., Yamaoka, H., Kumagai, S., & Shigeyama, T. 1994, *ApJ*, 437, L115
- Jha, S., et al. 1999, *ApJS*, 125, 73
- Krisciunas, K., Hastings, N. C., Loomis, K., McMillan, R., Rest, A., Riess, A. G., & Stubbs, C. 2000, *ApJ*, 539, 658
- Landolt, A. U. 1992, *AJ*, 104, 340
- Leibundgut, B., Tammann, G. A., Cadonau, R., & Cerrito, D. 1991, *A&AS*, 89, 537
- Lira, P. 1995, M.S. thesis, University of Chile
- Martin, R., Williams, A., & Woodings, S. 1999, *IAU Circ.* 7310
- Maza, J., Wischnjewsky, M., Torres, C., González, L., Costa, E., & Wroblewski, H. 1981, *PASP*, 93, 239
- Maza, J., Hamuy, M., Wischnjewsky, M., González, L., Candia, P., & Lidman, C. 1999, *IAU Circ.* 7272
- Meikle, W. P. S. 2000, *MNRAS*, 314, 782
- Menzies, J. W. 1989, *MNRAS*, 237, 21
- Munari, U., & Zwitter, T. 1997, *A&A*, 318, 269
- Nomoto, K., Yamaoka, H., Pols, O. R., van den Heuvel, E. P. J., Iwamoto, K., Kumakai, S., & Shigeyama, T. 1994, *Nature*, 371, 227
- Phillips, M. M., Lira, P., Suntzeff, N. B., Schommer, R. A., Hamuy, M., & Maza, J. 1999, *AJ*, 118, 1766
- Pinto, P. A., & Eastman, R. G. 2000, *ApJ*, 530, 757
- Richmond, M. W., Treffers, R. R., Filippenko, A. V., Paik, Y., Leibundgut, B., Schulman, E., & Cox, C. V. 1994, *AJ*, 107, 1022

- Richmond, M. W., et al. 1996, *AJ*, 111, 327
- Riess, A. G., Press, W. H., & Kirshner, R. P. 1996, *ApJ*, 473, 88
- Schlegel, D. J., Finkbeiner, D. P., & Davis, M. 1998, *ApJ*, 500, 525
- Schmidt, B. P., et al. 1993, *Nature*, 364, 600
- Schneider, D. P., Gunn, J. E., & Hoessel, J. G., 1983, *ApJ*, 264, 337
- Shigeyama, T., Nomoto, K., Tsujimoto, T., & Hashimoto, M. 1990, *ApJ*, 361, L23
- Sramek, R. A., Panagia, N., & Weiler, K. W. 1984, *ApJ*, 285, L59
- Suntzeff, N. B., Hamuy, M., Martin, G., Gómez, A., & González, R. 1988, *AJ*, 96, 1864
- Suntzeff, N. B., & Bouchet, P. 1990, *AJ*, 99, 650
- Suntzeff, N. B., et al. 1999, *AJ*, 117, 1175
- Suntzeff, N. B. 2000, in *Cosmic Explosions, Tenth Astrophysics Conference*, ed. S.S. Holt, & W.W. Zhang (AIP, New York), 65
- Strolger, L. G., et al. 1999, *BAAS*, 195, 3801
- Woosley, S. E., Pinto, P. A., Martin, P. G., & Weaver, T. A. 1987, *ApJ*, 318, 664
- Woosley, S. E., Langer, N., Weaver, T. A. 1993, *ApJ*, 411, 823
- Woosley, S. E., Langer, N., Weaver, T. A. 1995, *ApJ*, 448, 315

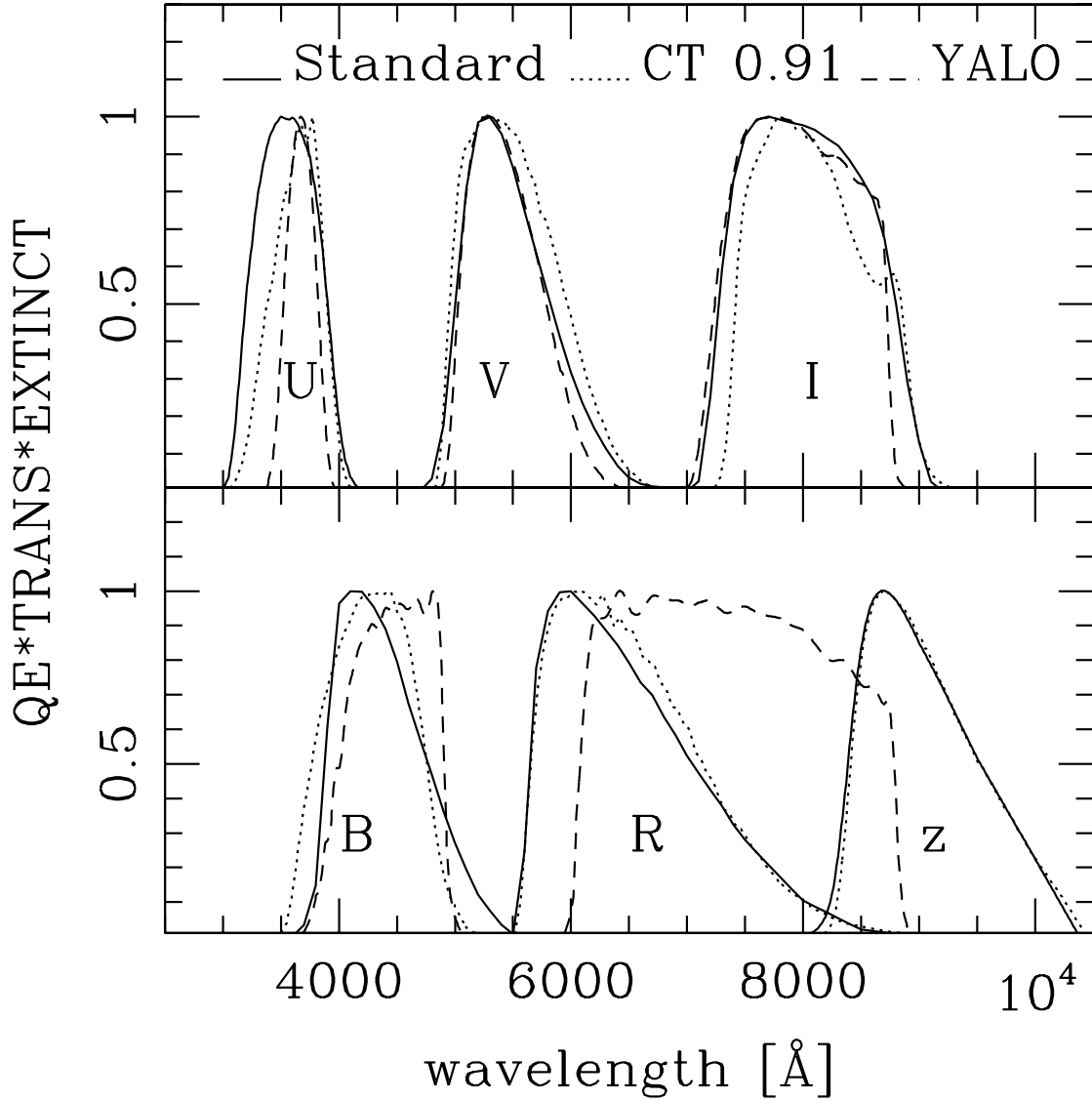


Fig. 1.— Comparison of *UBVRIZ* bandpasses for the YALO (dashed line) and CTIO 0.91-m (dotted line) telescopes. Each of these curves corresponds to the multiplication of the filter transmission curve, CCD quantum efficiency, and the atmospheric continuum transmission spectrum for one airmass. Atmospheric line opacity is not included in these bandpasses because they are used with spectra containing telluric lines. Also shown (solid line) are the Bessell (1990) standard Johnson/Kron-Cousins functions and the standard *z* function defined by Hamuy et al. (2001).

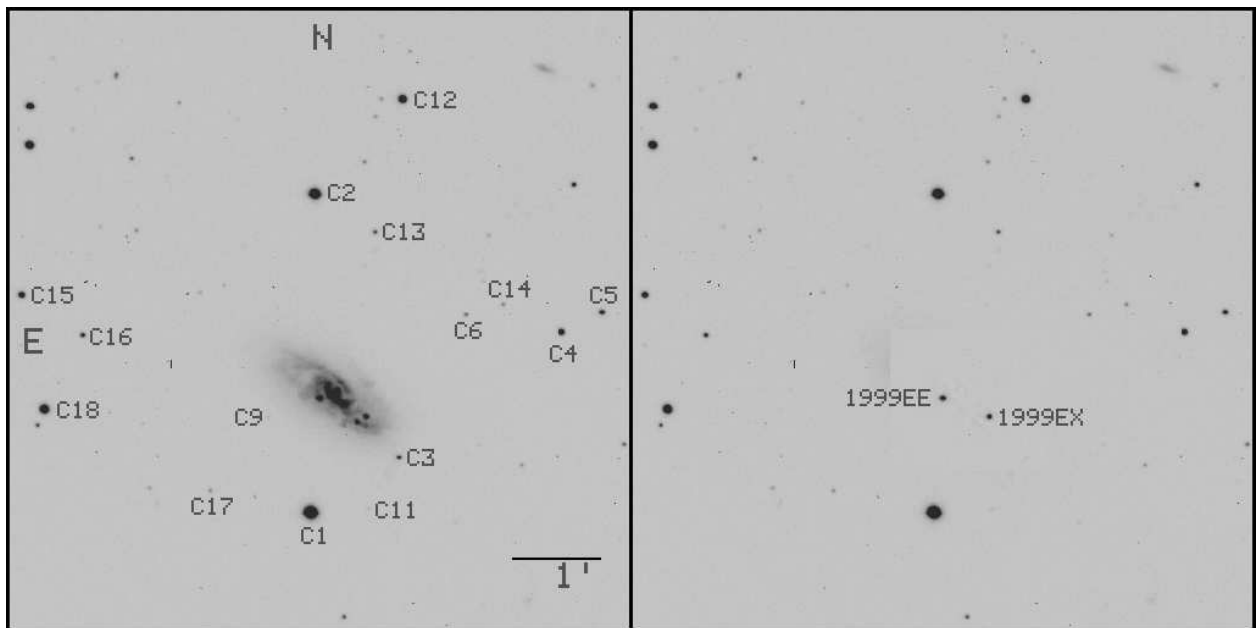


Fig. 2.— *V* band CCD image of SN 1999ee and SN 1999ex in IC 5179 taken on 1999 Nov. 17. The photometric sequence stars are labeled. The right panel displays the galaxy subtracted image clearly revealing both SNe. To avoid subtracting the local photometric sequence from the subtracted image we restricted the subtraction to the image section around the host galaxy.

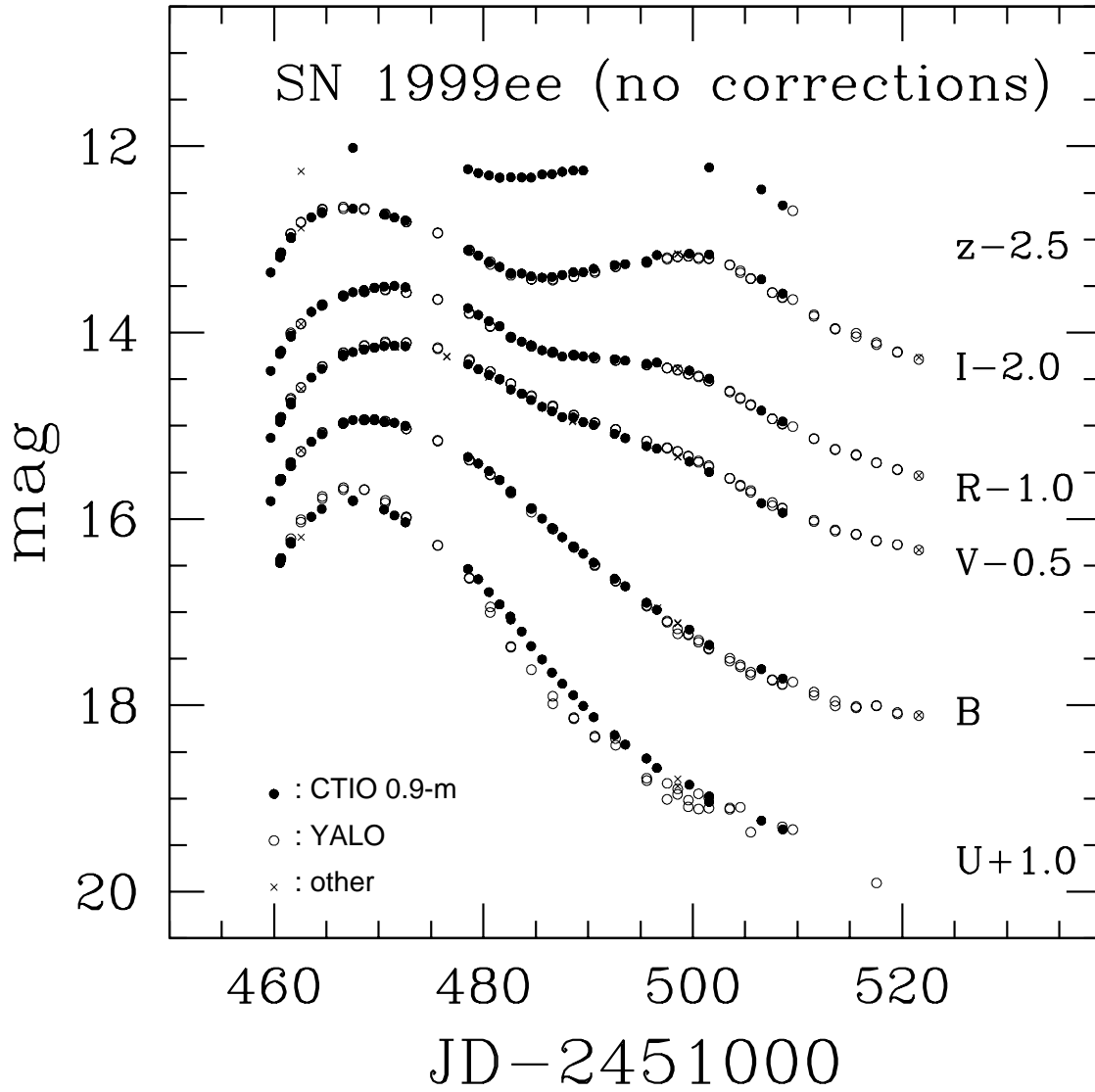


Fig. 3.— *UBVRIz* lightcurves of SN 1999ee. Open points and closed points show photometry from the YALO and CTIO 0.91-m telescopes, respectively.

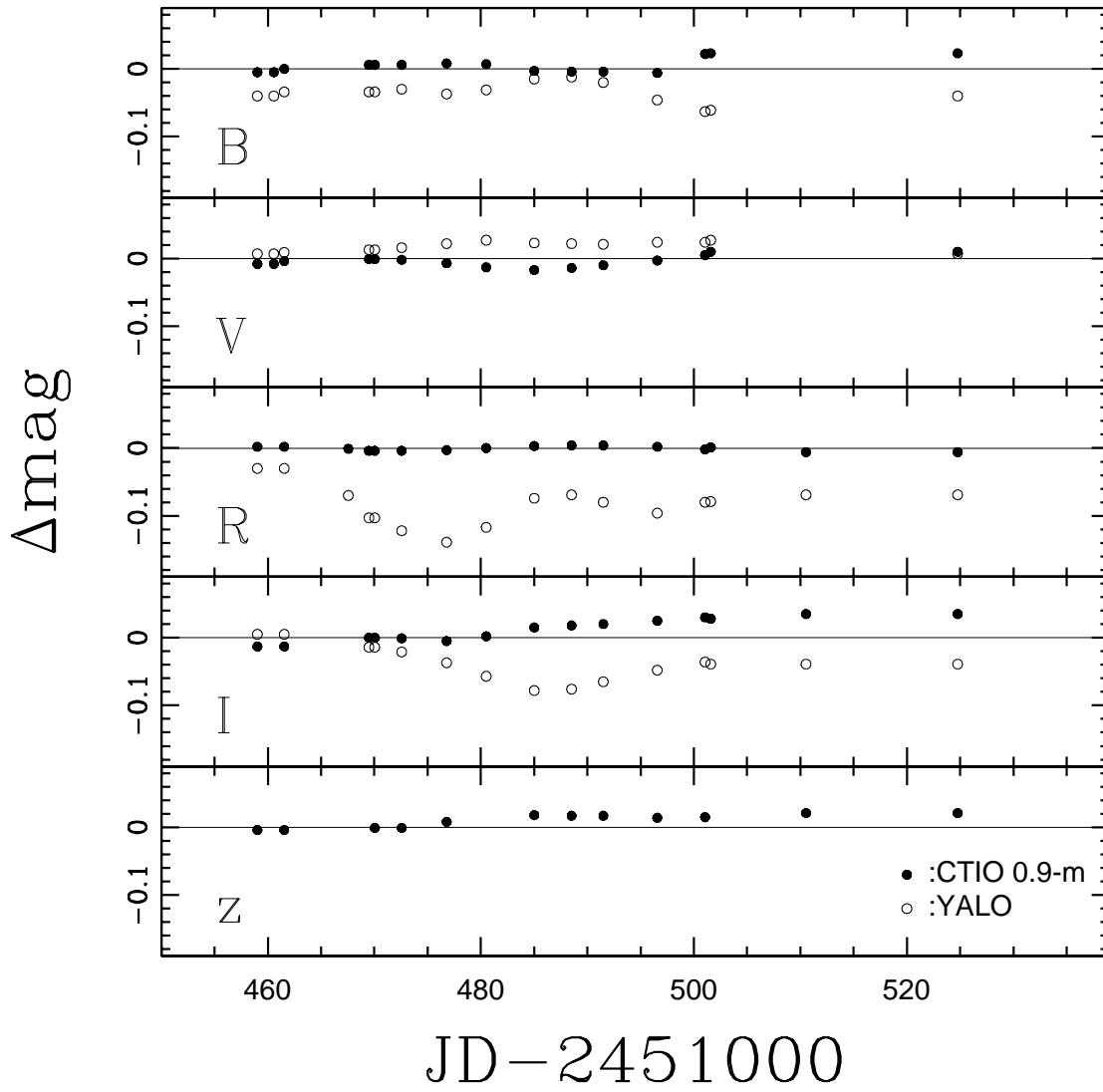


Fig. 4.— S-corrections as a function of Julian Date for SN 1999ee, computed from the YALO (open points) and CTIO 0.91-m (closed points).

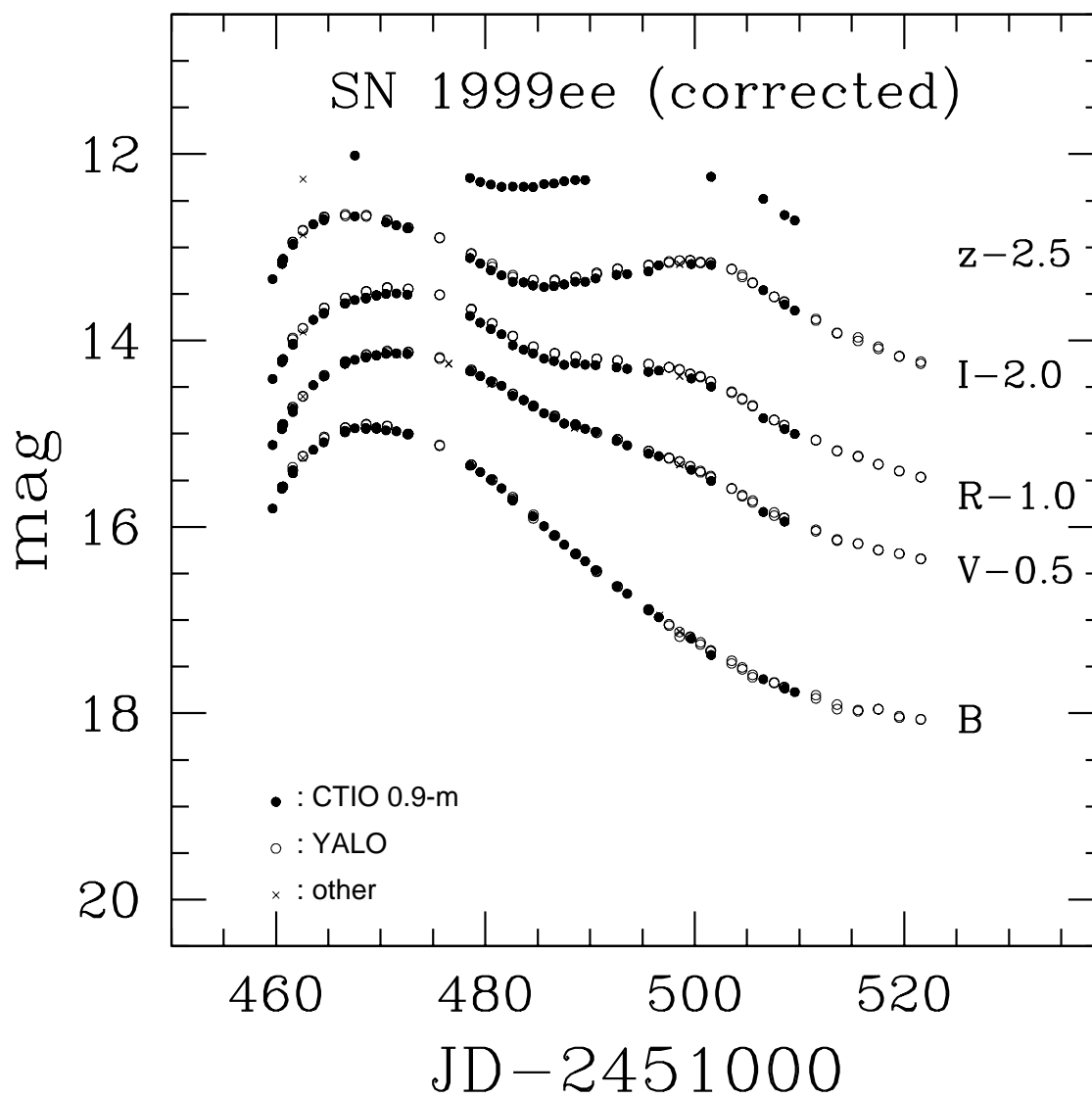


Fig. 5.— *UBVRIz* lightcurves of SN 1999ee after applying S-corrections. Open points and closed points show photometry from the YALO and CTIO 0.91-m telescopes, respectively.

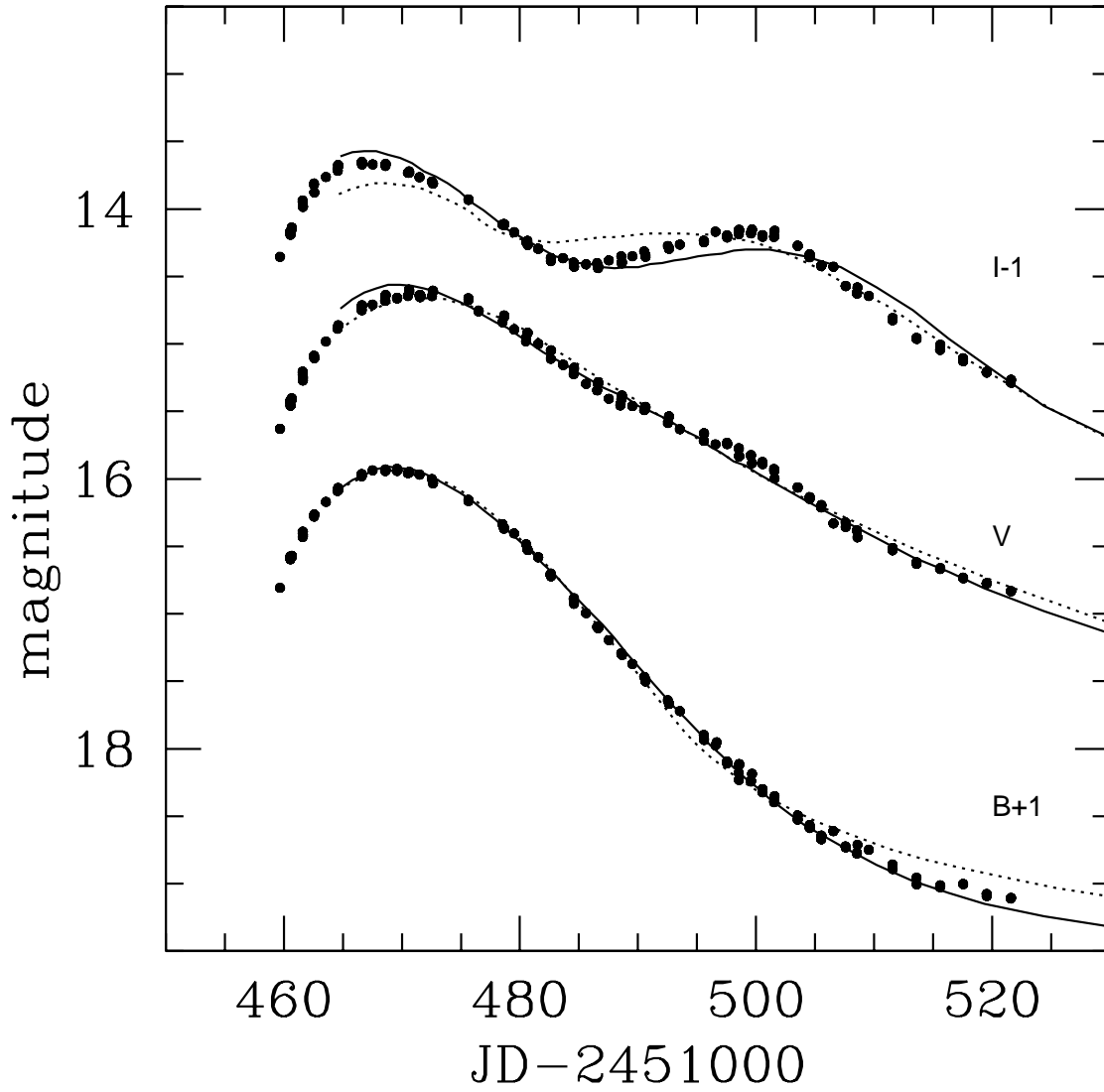


Fig. 6.— Template fitting for SN 1999ee. Solid line is SN 1992bc and dashed line is SN 1991T, both modified for time dilation and K correction for the corresponding redshift of SN 1999ee.

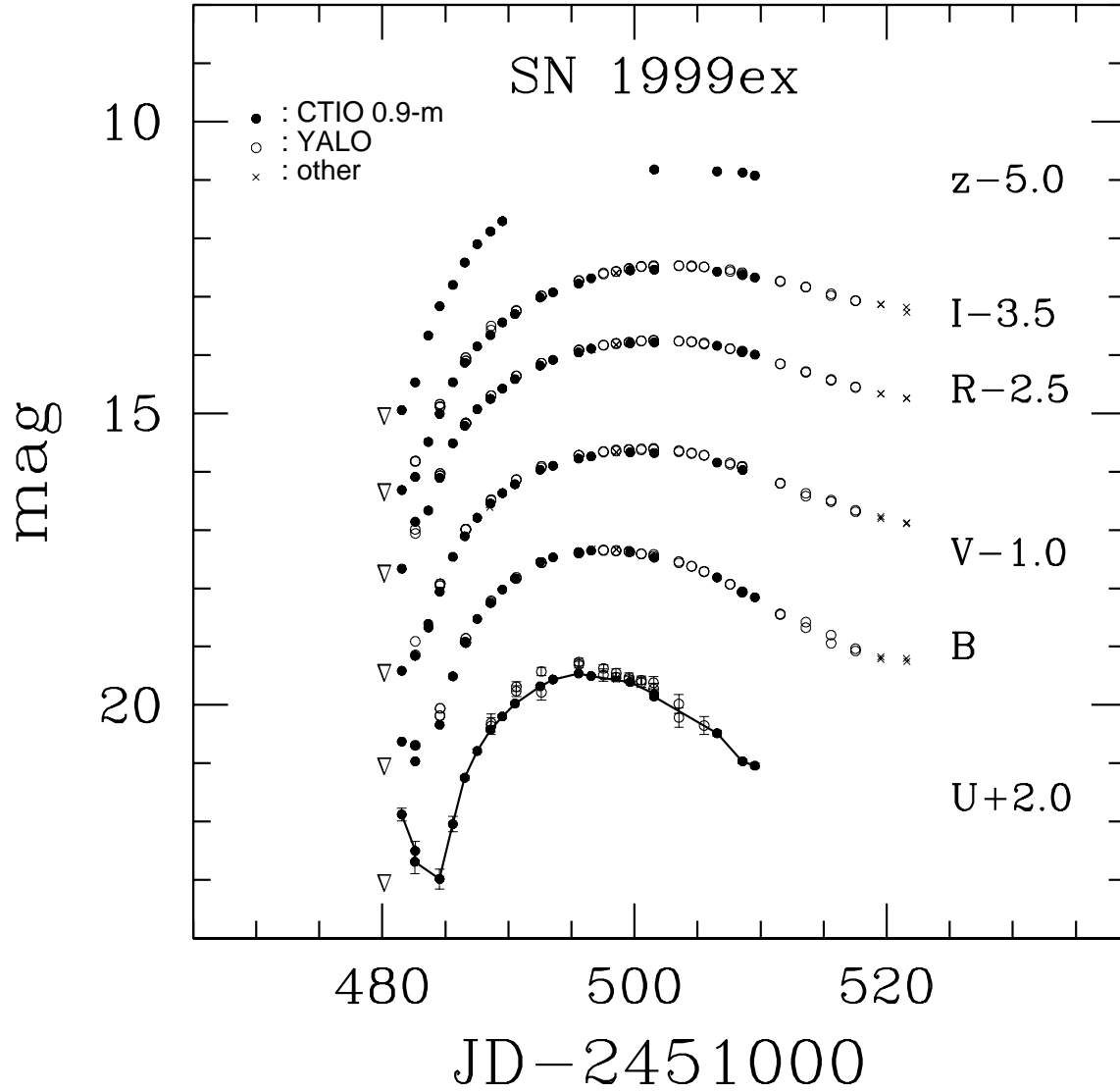


Fig. 7.— *UBVRIz* lightcurves of SN 1999ex. Open points and closed points show photometry from the YALO and CTIO 0.91-m telescopes, respectively. Upper limits derived from images taken on JD 2,451,480.5 are also included. The solid line through the *U* data is drawn to help the eye to see the initial upturn.

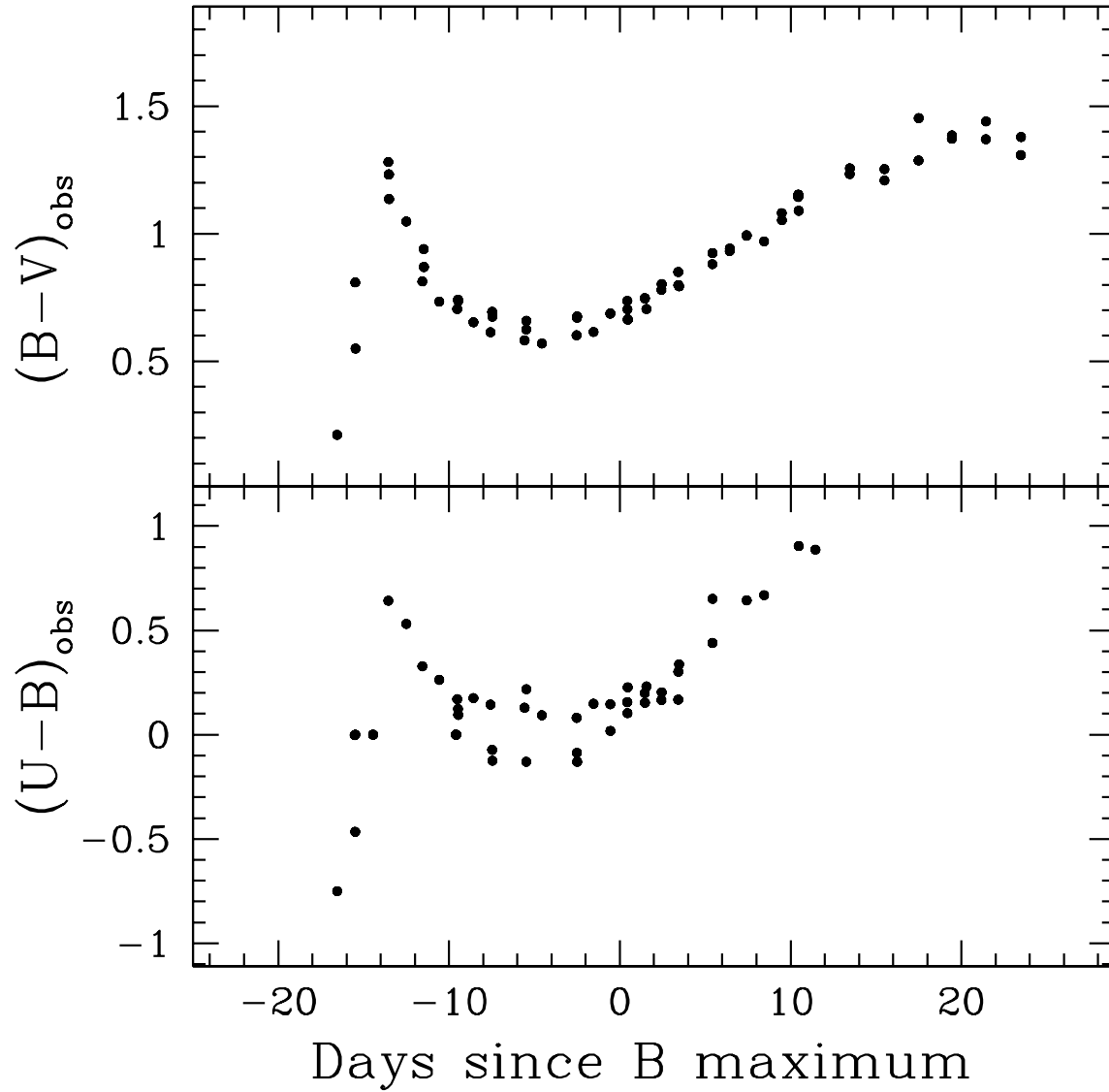


Fig. 8.— $B - V$ and $U - B$ color curves of SN 1999ex as a function of time since B maximum.

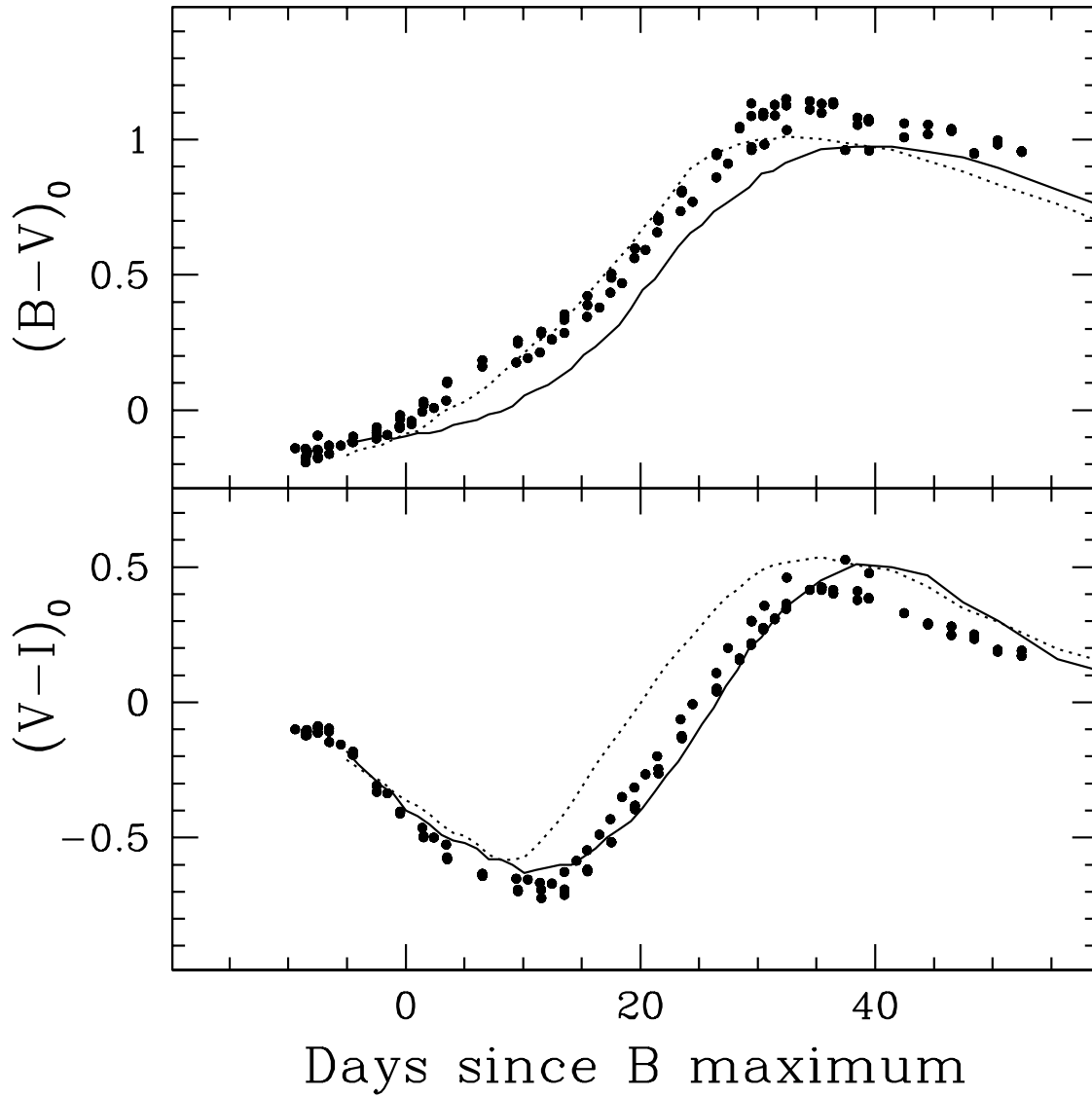


Fig. 9.— $(B-V)_0$ and $(V-I)_0$ color curves of SN 1999ee as a function of time since B maximum. For comparison are shown the templates curves of SN 1992bc (solid line) and SN 1991T (dotted line).

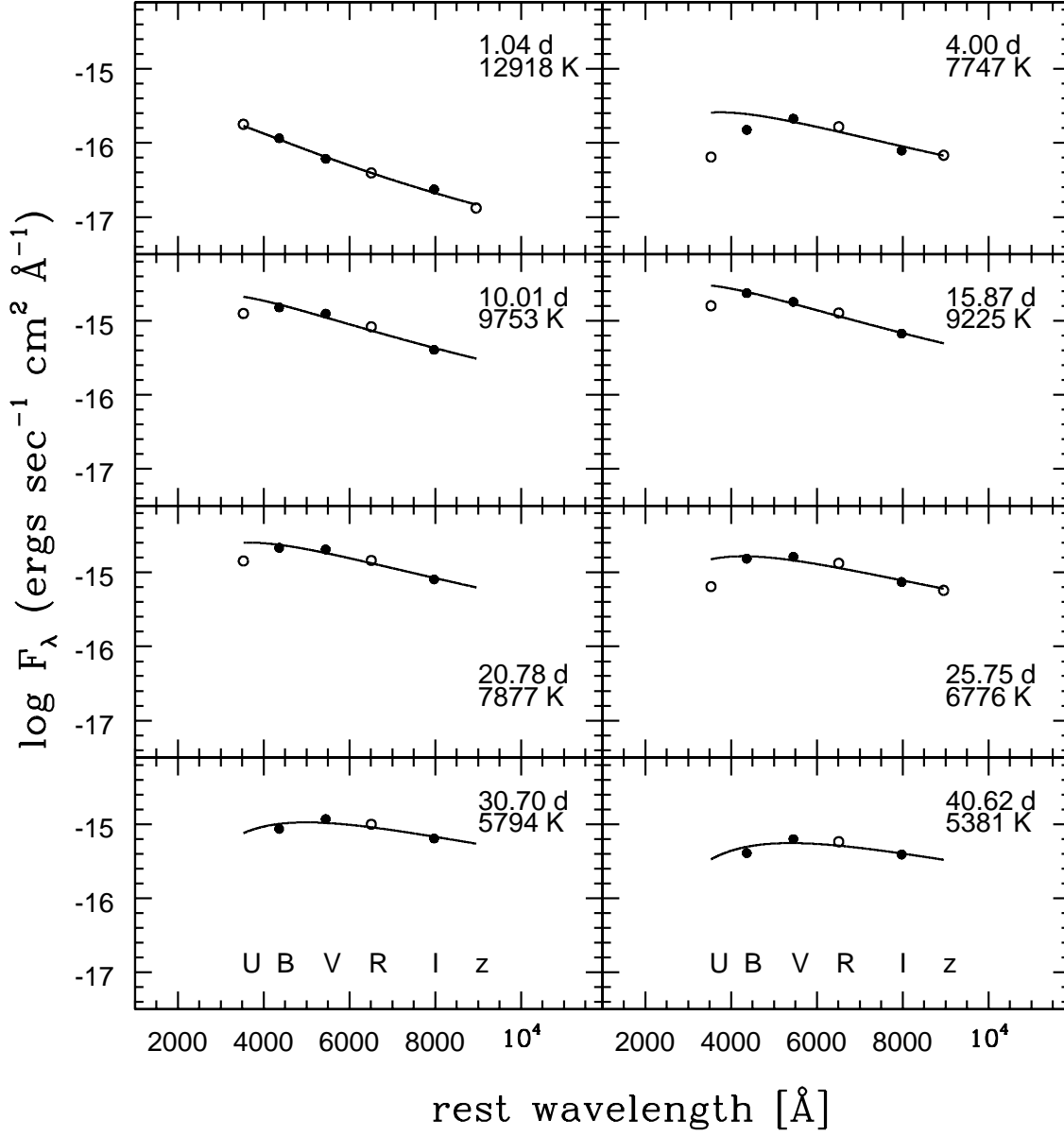


Fig. 10.— Blackbody fits to the BVI magnitudes (closed circles) of SN 1999ex for eight representative epochs (measured since explosion time). The URz magnitudes are also shown (open circles) but they were not included in the fits. Although the fits were done by converting BB fluxes into broad-band Vega magnitudes, for plotting purposes the SN magnitudes were converted into monochromatic fluxes (assuming $E(B - V)_{Gal}=0.02$ and $E(B - V)_{host}=0.28$).

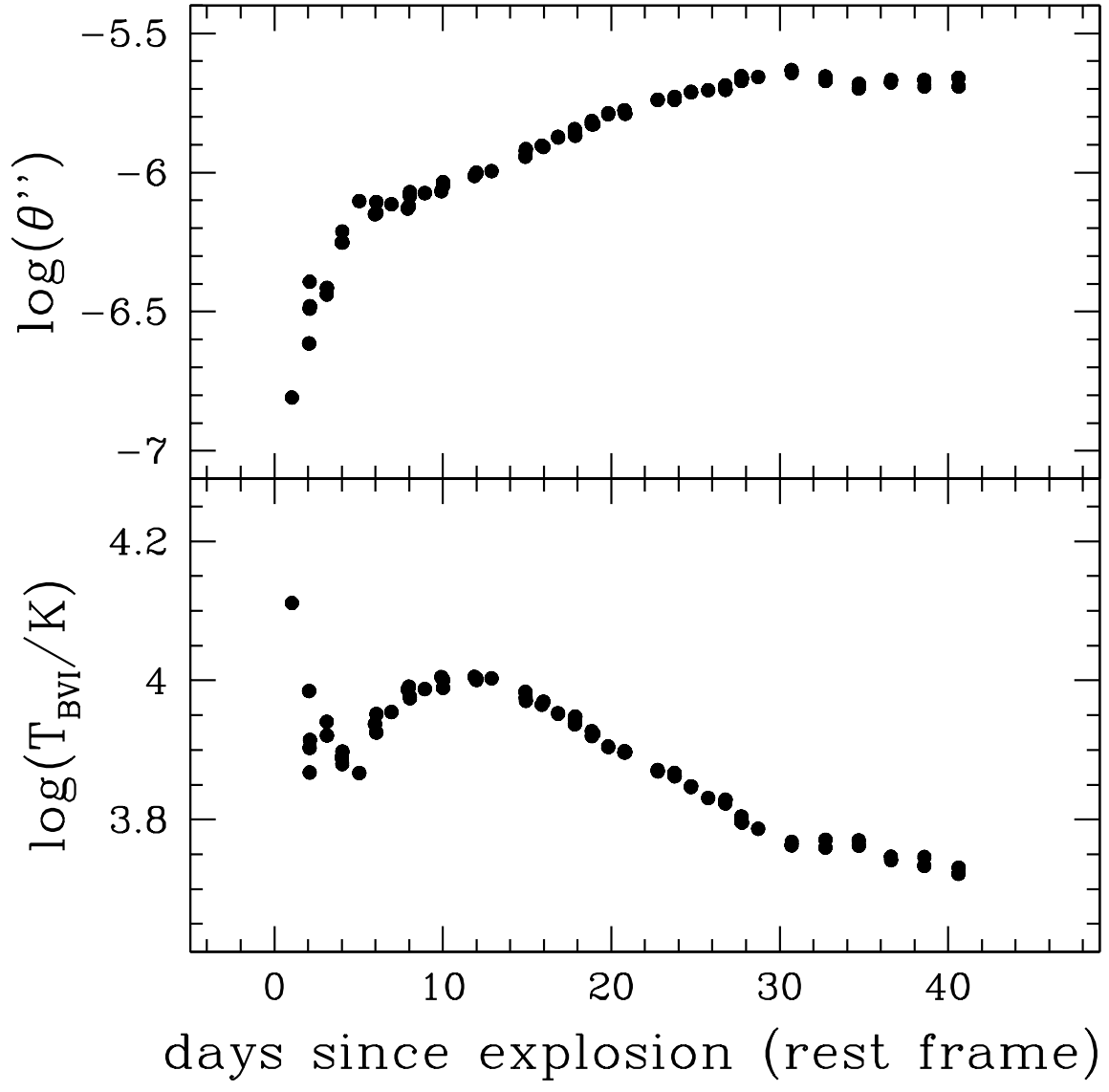


Fig. 11.— Angular radius and color temperature evolution of SN 1999ex derived from blackbody fits to the *BVI* magnitudes, assuming $E(B - V)_{Gal}=0.02$, $E(B - V)_{host}=0.28$, and JD 2,451,480.5 for the explosion time.

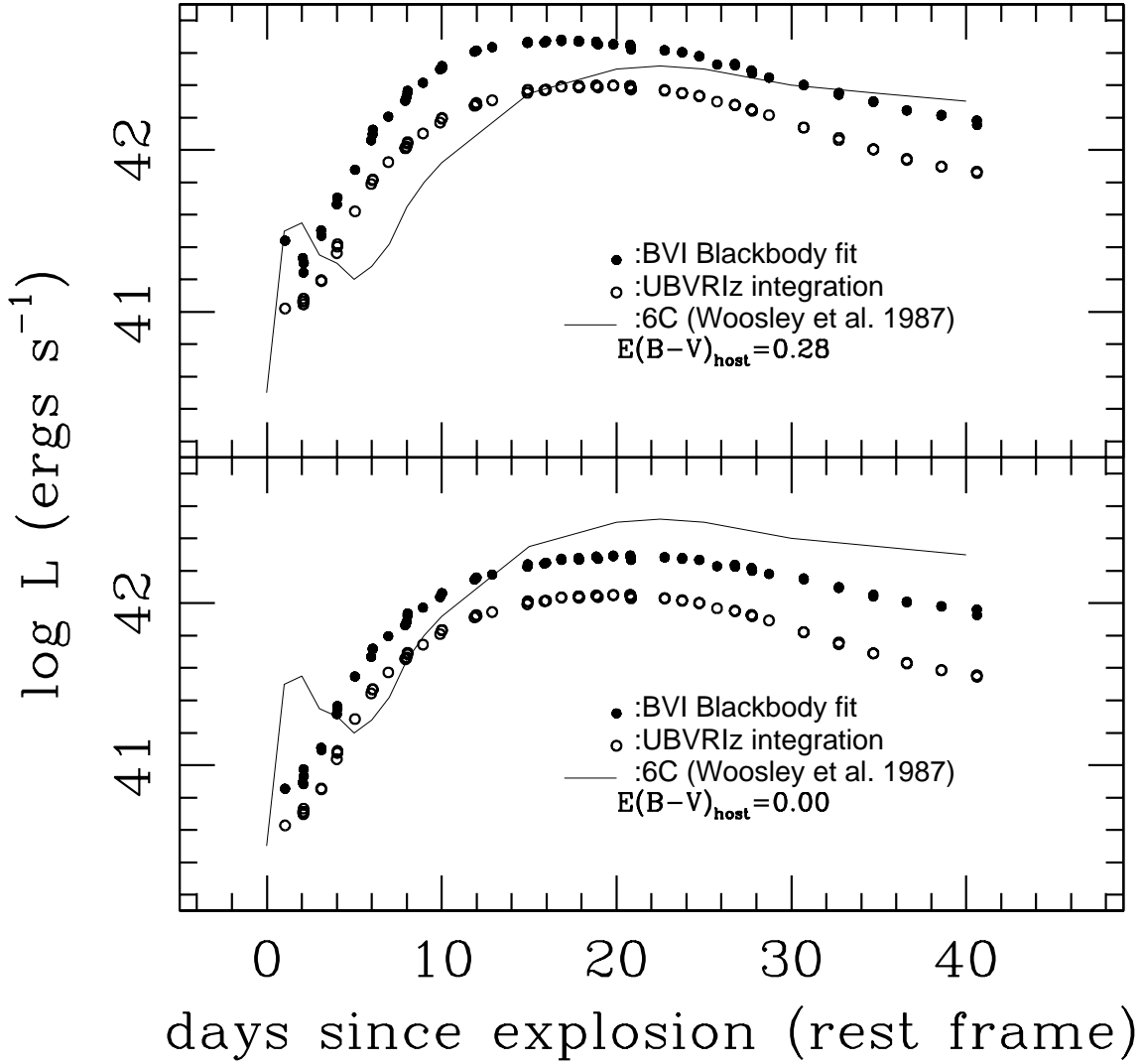


Fig. 12.— Bolometric lightcurve of SN 1999ex derived from blackbody fits to the *BVI* magnitudes (closed circles) and from a direct integration of the *UBVRIZ* fluxes (open points). The top panel assumes $E(B - V)_{\text{host}} = 0.28$ whereas the bottom panel adopts $E(B - V)_{\text{host}} = 0.00$. The solid line is the 6C hydrogenless core bounce SN model of Woosley et al. (1987).

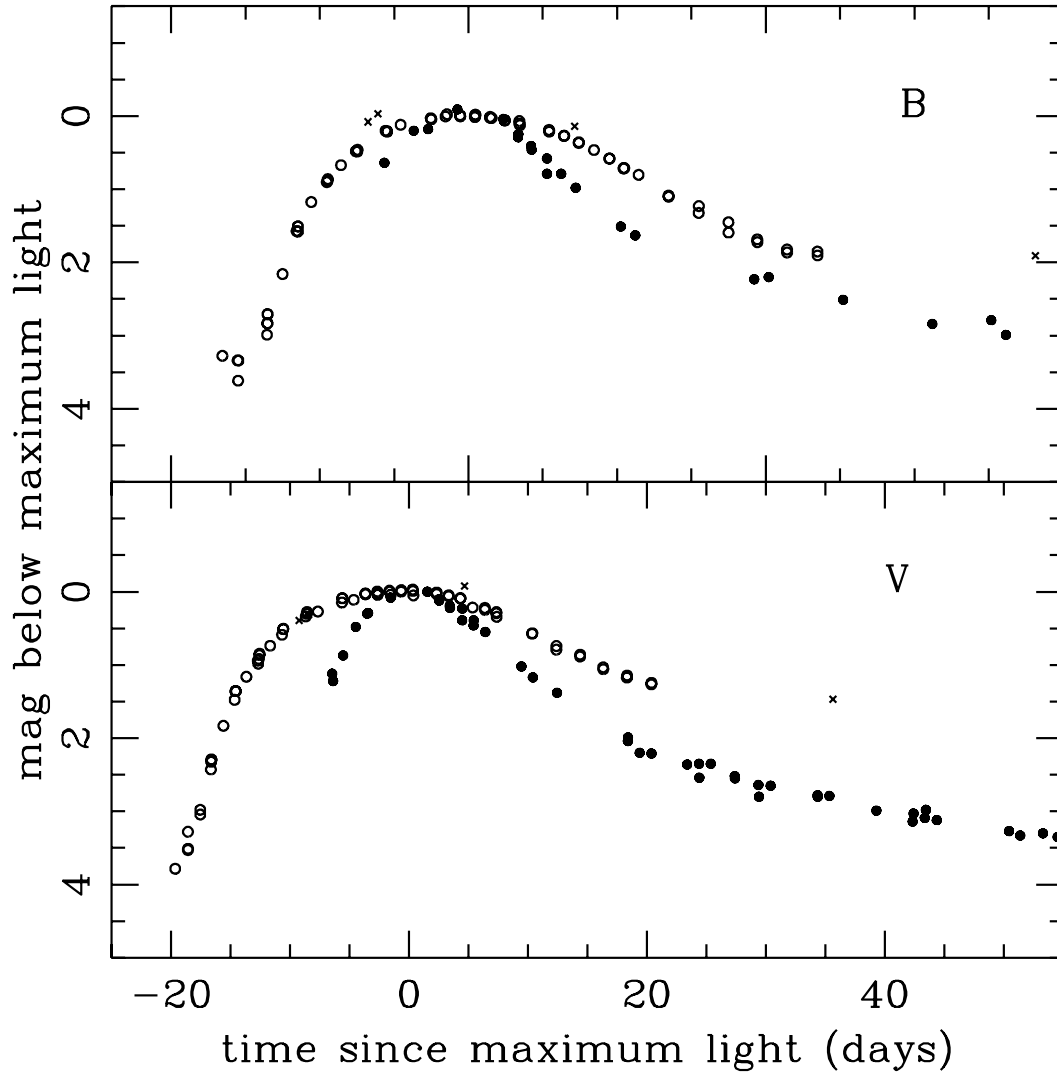


Fig. 13.— Comparison of the *B* and *V*-band lightcurves of SN 1999ex (open points), SN 1994I (closed points), and SN 1983V (crosses).

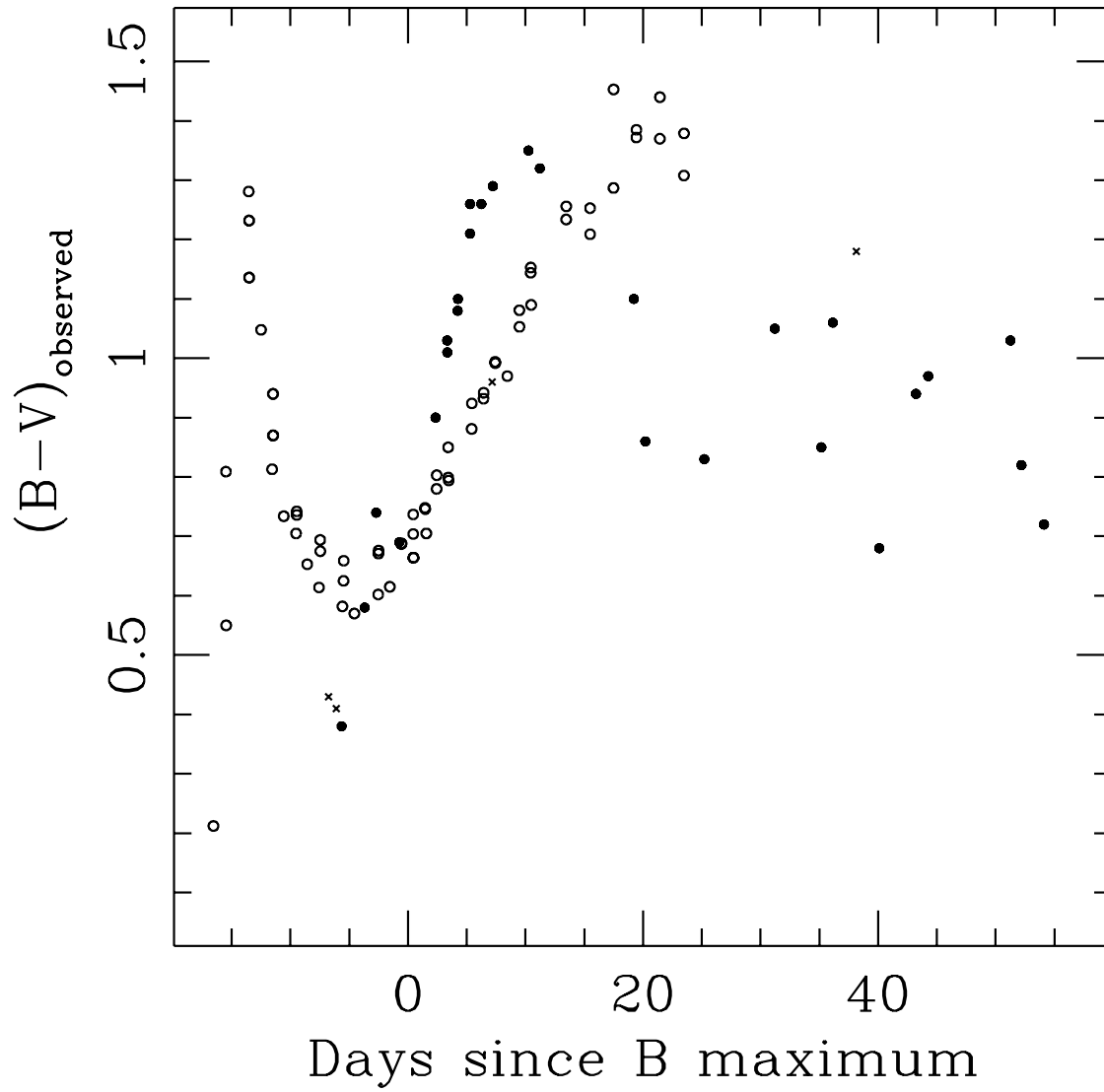


Fig. 14.— Comparison of the $B - V$ color curves of SN 1999ex (open points), SN 1994I (closed points), and SN 1983V (crosses).

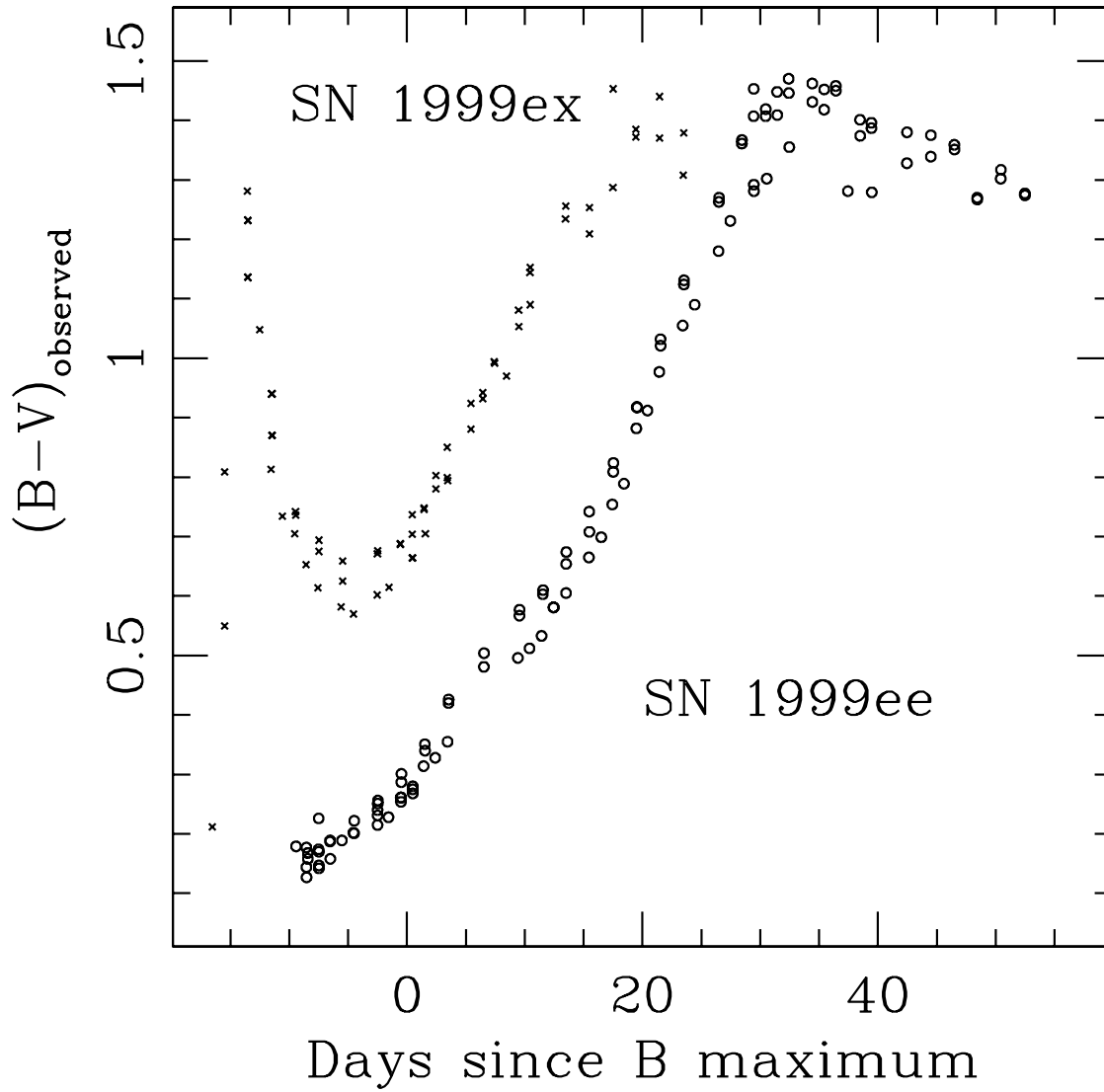


Fig. 15.— $B - V$ color curves of SN 1999ee (open circles) and SN 1999ex (crosses) as a function of time since B maximum.

Table 1. Journal of Observations

Date(UT)	Telescope	Observatory	Observer(s)
1999 Oct. 08	0.91-m	Tololo	Candia
1999 Oct. 09	0.91-m	Tololo	Stubbs
1999 Oct. 10	0.91-m	Tololo	Stubbs
1999 Oct. 10	YALO	Tololo	Service Observing
1999 Oct. 11	YALO	Tololo	Service Observing
1999 Oct. 11	NTT	La Silla	Hamuy/Doublier
1999 Oct. 11	NTT	La Silla	Hamuy/Doublier
1999 Oct. 12	0.91-m	Tololo	Candia
1999 Oct. 13	0.91-m	Tololo	Hamuy/Pérez
1999 Oct. 13	YALO	Tololo	Service Observing
1999 Oct. 15	0.91-m	Tololo	Becker/Stubbs
1999 Oct. 15	YALO	Tololo	Service Observing
1999 Oct. 16	0.91-m	Tololo	Hamuy/Acevedo
1999 Oct. 17	0.91-m	Tololo	Becker/Stubbs
1999 Oct. 17	YALO	Tololo	Service Observing
1999 Oct. 18	0.91-m	Tololo	Becker/Stubbs
1999 Oct. 19	0.91-m	Tololo	Strolger
1999 Oct. 19	YALO	Tololo	Service Observing
1999 Oct. 20	0.91-m	Tololo	Strolger
1999 Oct. 20	1.54-m	La Silla	Pompei/Joguet/Sekiguchi
1999 Oct. 21	0.91-m	Tololo	Strolger
1999 Oct. 21	YALO	Tololo	Service Observing
1999 Oct. 24	YALO	Tololo	Service Observing
1999 Oct. 25	1.54-m	La Silla	Augusteyn
1999 Oct. 27	0.91-m	Tololo	Hamuy/Wischnjewsky
1999 Oct. 27	YALO	Tololo	Service Observing
1999 Oct. 28	0.91-m	Tololo	Wischnjewsky
1999 Oct. 29	1.54-m	La Silla	Augusteyn
1999 Oct. 29	0.91-m	Tololo	Wischnjewsky
1999 Oct. 29	YALO	Tololo	Service Observing
1999 Oct. 30	0.91-m	Tololo	Wischnjewsky
1999 Oct. 31	0.91-m	Tololo	Wischnjewsky
1999 Oct. 31	YALO	Tololo	Service Observing

Table 1—Continued

Date(UT)	Telescope	Observatory	Observer(s)
1999 Nov. 01	0.91-m	Tololo	Wischnjewsky
1999 Nov. 02	0.91-m	Tololo	González
1999 Nov. 02	YALO	Tololo	Service Observing
1999 Nov. 03	0.91-m	Tololo	González
1999 Nov. 04	0.91-m	Tololo	González
1999 Nov. 04	YALO	Tololo	Service Observing
1999 Nov. 05	0.91-m	Tololo	González
1999 Nov. 06	0.91-m	Tololo	González
1999 Nov. 06	YALO	Tololo	Service Observing
1999 Nov. 06	1.54-m	La Silla	Augusteyn
1999 Nov. 07	0.91-m	Tololo	González
1999 Nov. 08	0.91-m	Tololo	Strolger
1999 Nov. 08	YALO	Tololo	Service Observing
1999 Nov. 10	0.91-m	Tololo	Strolger
1999 Nov. 10	YALO	Tololo	Service Observing
1999 Nov. 11	0.91-m	Tololo	Strolger
1999 Nov. 13	0.91-m	Tololo	Rubenstein
1999 Nov. 13	YALO	Tololo	Service Observing
1999 Nov. 14	NTT	La Silla	Hamuy/Doublier
1999 Nov. 14	NTT	La Silla	Hamuy/Doublier
1999 Nov. 14	0.91-m	Tololo	Strolger
1999 Nov. 15	YALO	Tololo	Service Observing
1999 Nov. 16	1.5-m	Tololo	Strolger
1999 Nov. 16	YALO	Tololo	Service Observing
1999 Nov. 17	0.91-m	Tololo	Rubenstein
1999 Nov. 17	YALO	Tololo	Service Observing
1999 Nov. 18	YALO	Tololo	Service Observing
1999 Nov. 19	0.91-m	Tololo	Strolger
1999 Nov. 19	YALO	Tololo	Service Observing
1999 Nov. 21	YALO	Tololo	Service Observing
1999 Nov. 22	YALO	Tololo	Service Observing
1999 Nov. 23	YALO	Tololo	Service Observing
1999 Nov. 24	0.91-m	Tololo	Hamuy/Antezana

Table 1—Continued

Date(UT)	Telescope	Observatory	Observer(s)
1999 Nov. 25	YALO	Tololo	Service Observing
1999 Nov. 26	0.91-m	Tololo	Antezana
1999 Nov. 26	YALO	Tololo	Service Observing
1999 Nov. 27	0.91-m	Tololo	Antezana
1999 Nov. 29	YALO	Tololo	Service Observing
1999 Dec. 01	YALO	Tololo	Service Observing
1999 Dec. 03	YALO	Tololo	Service Observing
1999 Dec. 05	YALO	Tololo	Service Observing
1999 Dec. 07	YALO	Tololo	Service Observing
1999 Dec. 09	YALO	Tololo	Service Observing
2001 Jul. 16	1.5-m	Tololo	Candia

Table 2. *UBVRIZ* Photometric Sequence Around IC 5179

Star	<i>U</i>	<i>B</i>	<i>V</i>	<i>R</i>	<i>I</i>	<i>z</i>
c1	14.282(012)	10.822(015)
c2	13.663(010)	12.361(043)
c3	19.579(043)	18.366(008)	16.866(009)	15.886(009)	14.793(009)	14.415(019)
c4	17.183(012)	16.649(013)	15.789(011)	15.278(011)	14.826(011)	14.625(032)
c5	18.985(035)	17.640(014)	16.334(015)	15.511(015)	14.817(015)	14.513(027)
c6	20.532(163)	19.445(018)	18.009(009)	17.061(011)	16.048(009)	15.666(028)
c9	...	21.366(240)	19.779(039)	18.830(062)	18.016(028)	17.574(057)
c11	19.803(087)	20.033(046)	19.525(031)	19.234(038)	18.944(067)	19.287(228)
c12	15.490(010)	15.418(008)	14.794(009)	14.407(011)	14.036(011)	13.880(025)
c13	18.047(013)	18.161(011)	17.613(010)	17.246(009)	16.891(009)	16.675(044)
c14	18.525(022)	18.701(010)	18.293(009)	18.011(009)	17.716(013)	17.545(014)
c15	16.940(010)	16.618(008)	15.860(009)	15.401(009)	15.012(009)	14.864(011)
c16	17.825(012)	17.695(008)	17.017(009)	16.616(009)	16.253(009)	16.087(024)
c17	...	19.727(022)	18.233(011)	17.061(013)	15.537(011)	14.957(035)
c18	14.761(015)	14.835(010)	14.346(011)	14.025(011)	13.707(011)	13.606(015)

Table 3. Color Terms for the Different Photometric Systems

Telescope	U	B	V	R	I	z
CTIO 0.9-m	+0.140	-0.083	+0.017	+0.019	+0.020	+0.007
YALO	+0.079	+0.098	-0.019	+0.352	-0.020	...
CTIO 1.54-m	+0.139	-0.080	+0.030	+0.016	+0.017	...
NTT	+0.061	-0.121	+0.020	+0.007	-0.035	0.000
D1.54-m	+0.033

Table 4. *UBVRIz* Photometry for SN 1999ee

JD-2,451,000	<i>U</i>	<i>B</i>	<i>V</i>	<i>R</i>	<i>I</i>	<i>z</i>	Method	Telescope
459.68	...	15.808(014)	15.629(015)	15.410(015)	15.354(015)	...	PHOT	CTIO 0.9-m
460.56	15.440(017)	15.575(014)	15.431(015)	15.221(015)	15.167(015)	...	PHOT	CTIO 0.9-m
460.56	15.462(017)	15.596(014)	15.419(015)	15.230(015)	15.166(015)	...	PHOT	CTIO 0.9-m
460.57	15.473(017)	15.585(014)	15.458(015)	15.210(015)	15.191(015)	...	PHOT	CTIO 0.9-m
460.68	15.419(017)	15.571(014)	15.403(015)	15.203(015)	15.149(015)	...	PHOT	CTIO 0.9-m
460.68	15.437(017)	15.570(014)	15.412(015)	15.197(015)	15.146(015)	...	PHOT	CTIO 0.9-m
460.68	15.422(017)	15.578(014)	15.410(015)	15.200(015)	15.137(015)	...	PHOT	CTIO 0.9-m
461.59	15.249(016)	15.394(017)	15.220(015)	15.019(011)	14.937(015)	...	DAO	YALO
461.60	15.212(016)	15.431(017)	15.205(015)	15.002(011)	14.942(015)	...	DAO	YALO
461.62	15.265(082)	15.413(014)	15.271(015)	15.033(015)	14.984(015)	...	PHOT	CTIO 0.9-m
461.62	15.247(017)	15.425(014)	15.255(015)	15.034(015)	14.976(015)	...	PHOT	CTIO 0.9-m
461.62	15.256(021)	15.392(014)	15.245(015)	15.044(015)	14.983(015)	...	PHOT	CTIO 0.9-m
462.56	15.033(016)	15.274(017)	15.087(015)	14.908(011)	14.820(015)	...	DAO	YALO
462.57	15.006(016)	15.279(017)	15.090(015)	14.904(011)	14.812(015)	...	DAO	YALO
462.59	15.195(016)	15.264(013)	15.106(015)	14.907(015)	14.878(016)	14.769(015)	PHOT	NTT
463.57	14.977(017)	15.171(014)	14.982(015)	14.777(015)	14.763(015)	...	PHOT	CTIO 0.9-m
464.55	14.892(017)	15.090(014)	14.888(015)	14.712(015)	14.705(015)	...	PHOT	CTIO 0.9-m
464.58	14.703(015)	14.717(015)	...	PHOT	CTIO 0.9-m
464.61	14.758(016)	15.068(017)	14.867(015)	14.703(011)	14.674(015)	...	PHOT	YALO
464.62	14.782(016)	15.083(017)	14.861(015)	14.699(011)	14.681(015)	...	PHOT	YALO
466.60	...	14.981(014)	14.750(015)	14.600(015)	PHOT	CTIO 0.9-m
466.60	...	14.965(014)	14.750(015)	14.605(015)	PHOT	CTIO 0.9-m
466.60	...	14.976(014)	14.736(015)	14.605(015)	PHOT	CTIO 0.9-m
466.62	14.685(016)	14.969(017)	14.718(015)	14.607(011)	14.651(015)	...	PHOT	YALO
466.63	14.664(016)	14.970(017)	14.714(015)	14.607(011)	14.670(015)	...	PHOT	YALO

Table 4—Continued

JD-2,451,000	<i>U</i>	<i>B</i>	<i>V</i>	<i>R</i>	<i>I</i>	<i>z</i>	Method	Telescope
467.53	14.807(017)	14.937(014)	14.709(015)	14.567(015)	14.670(015)	14.517(015)	PHOT	CTIO 0.9-m
467.54	14.802(017)	PHOT	CTIO 0.9-m
467.54	14.804(017)	PHOT	CTIO 0.9-m
468.59	...	14.934(014)	14.680(015)	14.544(015)	PHOT	CTIO 0.9-m
468.59	...	14.940(014)	14.679(015)	14.545(015)	PHOT	CTIO 0.9-m
468.59	...	14.942(014)	14.681(015)	14.553(015)	PHOT	CTIO 0.9-m
468.62	14.683(018)	14.931(017)	14.644(015)	14.563(011)	14.680(015)	...	DAO	YALO
468.63	14.687(016)	14.938(017)	14.637(015)	14.561(011)	14.666(015)	...	DAO	YALO
469.59	...	14.941(014)	14.661(015)	14.517(015)	PHOT	CTIO 0.9-m
469.60	...	14.926(014)	14.658(015)	14.523(015)	PHOT	CTIO 0.9-m
469.60	...	14.938(014)	14.663(015)	14.520(015)	PHOT	CTIO 0.9-m
470.51	14.899(017)	14.958(014)	14.644(015)	14.505(015)	14.733(015)	...	PHOT	CTIO 0.9-m
470.62	14.826(016)	14.948(017)	14.597(015)	14.535(011)	14.721(015)	...	DAO	YALO
470.63	14.801(032)	14.953(017)	14.613(015)	14.544(011)	14.733(015)	...	DAO	YALO
471.50	14.962(017)	14.968(014)	14.640(015)	14.498(015)	14.765(015)	...	PHOT	CTIO 0.9-m
471.54	14.653(015)	PHOT	D 1.54-m
471.55	14.652(015)	PHOT	D 1.54-m
471.55	14.637(015)	PHOT	D 1.54-m
471.59	14.647(015)	PHOT	D 1.54-m
472.55	15.036(017)	15.001(014)	14.646(015)	14.513(015)	14.797(015)	...	PHOT	CTIO 0.9-m
472.63	14.977(016)	15.032(017)	14.612(015)	14.569(011)	14.810(015)	...	DAO	YALO
472.64	14.988(018)	15.032(017)	14.606(015)	14.569(011)	14.811(015)	...	DAO	YALO
475.63	15.281(018)	15.155(017)	14.674(015)	14.645(011)	14.933(015)	...	DAO	YALO
475.64	15.284(017)	15.165(017)	14.661(015)	14.642(011)	14.928(015)	...	DAO	YALO
476.50	14.759(015)	PHOT	D 1.54-m

Table 4—Continued

JD-2,451,000	<i>U</i>	<i>B</i>	<i>V</i>	<i>R</i>	<i>I</i>	<i>z</i>	Method	Telescope
476.51	14.753(015)	PHOT	D 1.54-m
478.52	15.536(017)	15.335(014)	14.839(015)	14.738(015)	15.116(015)	14.746(015)	PHOT	CTIO 0.9-m
478.65	15.628(019)	15.369(017)	14.802(015)	14.797(011)	15.120(015)	...	DAO	YALO
478.66	15.638(021)	15.365(017)	14.788(015)	14.788(011)	15.111(015)	...	DAO	YALO
479.51	15.646(017)	15.405(014)	14.893(015)	14.810(015)	15.173(015)	14.787(015)	PHOT	CTIO 0.9-m
480.50	14.981(015)	PHOT	D 1.54-m
480.53	15.784(017)	15.486(014)	14.953(015)	14.877(015)	15.245(015)	14.813(015)	PHOT	CTIO 0.9-m
480.64	16.003(027)	15.521(017)	14.918(015)	14.934(011)	15.236(015)	...	DAO	YALO
480.66	15.943(096)	15.528(017)	14.918(015)	14.931(011)	15.267(015)	...	DAO	YALO
481.55	15.918(017)	15.581(014)	15.000(015)	14.932(015)	15.295(015)	14.837(015)	DAO	CTIO 0.9-m
481.55	15.918(017)	15.581(014)	15.000(015)	14.932(015)	15.295(015)	14.837(015)	DAO	CTIO 0.9-m
482.58	16.047(017)	15.709(014)	DAO	CTIO 0.9-m
482.61	16.078(017)	15.715(014)	15.110(015)	15.050(015)	15.362(015)	14.833(015)	DAO	CTIO 0.9-m
482.62	16.366(051)	15.703(017)	15.049(015)	15.047(011)	15.386(015)	...	DAO	YALO
482.63	16.377(090)	15.722(017)	15.048(015)	15.052(011)	15.365(015)	...	DAO	YALO
483.65	16.207(017)	...	15.154(015)	15.097(015)	15.365(015)	14.834(015)	DAO	CTIO 0.9-m
483.66	15.156(015)	DAO	CTIO 0.9-m
484.55	16.365(017)	15.889(014)	15.224(015)	15.135(015)	15.396(015)	14.836(015)	DAO	CTIO 0.9-m
484.58	16.617(040)	15.926(017)	15.184(015)	15.147(011)	15.427(015)	...	DAO	YALO
484.59	...	15.885(017)	15.177(015)	15.143(011)	15.427(015)	...	DAO	YALO
485.60	16.507(017)	15.995(014)	15.296(015)	15.190(015)	15.410(015)	14.803(015)	DAO	CTIO 0.9-m
486.54	16.648(017)	16.098(014)	15.344(015)	15.217(015)	15.401(015)	14.798(015)	DAO	CTIO 0.9-m
486.62	16.902(050)	16.105(017)	15.296(015)	15.212(011)	15.438(015)	...	DAO	YALO
486.63	16.982(066)	16.107(017)	15.283(015)	15.208(011)	15.425(015)	...	DAO	YALO
487.53	16.768(017)	16.195(014)	15.406(015)	15.257(015)	15.381(015)	14.774(015)	DAO	CTIO 0.9-m

Table 4—Continued

JD-2,451,000	<i>U</i>	<i>B</i>	<i>V</i>	<i>R</i>	<i>I</i>	<i>z</i>	Method	Telescope
488.50	15.456(015)	DAO	D 1.54-m
488.53	15.442(015)	PHOT	D 1.54-m
488.58	16.891(017)	16.293(014)	15.411(015)	15.240(015)	15.351(015)	14.761(015)	DAO	CTIO 0.9-m
488.63	17.131(051)	16.300(017)	15.382(015)	15.241(011)	15.402(015)	...	DAO	YALO
488.64	17.144(056)	16.304(017)	15.387(015)	15.243(011)	15.394(015)	...	DAO	YALO
489.53	17.006(017)	16.372(014)	15.460(015)	15.255(018)	15.351(015)	14.761(015)	DAO	CTIO 0.9-m
490.53	17.126(017)	16.468(014)	15.491(015)	15.261(016)	15.315(015)	...	DAO	CTIO 0.9-m
490.63	17.330(054)	16.501(017)	15.469(015)	15.273(011)	15.340(015)	...	DAO	YALO
490.64	17.344(067)	16.488(017)	15.467(015)	15.273(011)	15.355(015)	...	DAO	YALO
492.52	17.319(017)	16.641(014)	15.586(015)	15.284(015)	15.274(015)	...	DAO	CTIO 0.9-m
492.62	17.356(058)	16.664(017)	15.540(015)	15.299(011)	15.289(015)	...	DAO	YALO
492.63	17.427(094)	16.668(017)	15.537(015)	15.297(011)	15.295(015)	...	DAO	YALO
493.54	17.421(017)	16.722(014)	15.632(015)	15.301(015)	15.264(015)	...	DAO	CTIO 0.9-m
495.57	17.570(021)	16.898(014)	15.718(015)	15.334(015)	15.235(015)	...	DAO	CTIO 0.9-m
495.59	17.781(079)	16.925(017)	15.662(015)	15.345(011)	15.247(015)	...	DAO	YALO
495.60	17.807(106)	16.935(017)	15.665(015)	15.347(011)	15.239(015)	...	DAO	YALO
496.56	17.672(017)	16.975(014)	15.744(015)	15.321(015)	15.168(015)	...	DAO	CTIO 0.9-m
496.66	...	16.952(013)	...	15.330(015)	PHOT	NTT
497.54	18.008(154)	17.094(017)	15.733(015)	15.379(011)	15.196(015)	...	DAO	YALO
497.55	17.837(095)	17.109(017)	15.742(015)	15.380(011)	15.211(015)	...	DAO	YALO
498.54	17.866(017)	PHOT	CTIO 1.5-m
498.54	17.954(109)	17.180(017)	15.773(015)	15.398(011)	15.186(015)	...	DAO	YALO
498.55	17.897(120)	17.231(017)	15.778(015)	15.404(011)	15.185(015)	...	DAO	YALO
498.56	17.790(024)	17.122(014)	15.830(015)	15.381(015)	15.154(015)	...	PHOT	CTIO 1.5-m
498.57	...	17.114(014)	15.833(015)	15.386(015)	15.159(015)	...	PHOT	CTIO 1.5-m

Table 4—Continued

JD-2,451,000	<i>U</i>	<i>B</i>	<i>V</i>	<i>R</i>	<i>I</i>	<i>z</i>	Method	Telescope
499.56	18.089(090)	17.235(017)	15.828(015)	15.446(011)	15.178(015)	...	DAO	YALO
499.57	18.018(107)	17.243(017)	15.824(015)	15.442(011)	15.181(015)	...	DAO	YALO
499.66	17.852(023)	17.186(014)	15.884(015)	15.408(015)	15.152(015)	...	DAO	CTIO 0.9-m
500.54	17.949(093)	17.323(017)	15.875(015)	15.464(011)	15.193(015)	...	DAO	YALO
500.55	18.112(131)	17.300(017)	15.891(015)	15.476(011)	15.206(015)	...	DAO	YALO
501.52	17.988(134)	17.397(017)	15.927(015)	15.517(011)	15.207(015)	...	DAO	YALO
501.53	18.103(128)	17.387(017)	15.941(015)	15.520(011)	15.202(015)	...	DAO	YALO
501.55	18.037(030)	DAO	CTIO 0.9-m
501.57	17.976(031)	17.352(014)	15.997(015)	15.494(015)	15.161(015)	14.728(015)	DAO	CTIO 0.9-m
503.52	18.115(172)	17.525(017)	16.063(015)	15.624(011)	15.272(015)	...	DAO	YALO
503.53	18.100(152)	17.495(017)	16.064(015)	15.638(011)	15.274(015)	...	DAO	YALO
504.53	18.093(147)	17.566(017)	16.148(015)	15.709(011)	15.358(015)	...	DAO	YALO
504.54	...	17.587(017)	16.135(015)	15.697(011)	15.335(015)	...	DAO	YALO
505.52	...	17.671(018)	16.213(015)	15.781(011)	15.423(015)	...	DAO	YALO
505.53	18.361(155)	17.644(018)	16.194(015)	15.771(011)	15.417(015)	...	DAO	YALO
506.55	18.237(040)	17.611(014)	16.330(015)	15.837(017)	15.428(015)	14.963(016)	DAO	CTIO 0.9-m
507.58	...	17.724(020)	16.323(015)	15.925(011)	15.570(015)	...	DAO	YALO
507.59	...	17.731(023)	16.357(015)	15.925(011)	15.571(015)	...	DAO	YALO
508.54	18.302(113)	17.777(017)	16.381(015)	15.978(011)	15.620(015)	...	DAO	YALO
508.55	...	17.772(017)	16.385(015)	15.982(011)	15.627(015)	...	DAO	YALO
508.58	18.331(030)	17.712(014)	16.433(015)	15.954(015)	15.581(015)	15.134(015)	DAO	CTIO 0.9-m
509.55	18.333(027)	17.749(014)	...	16.008(015)	15.644(015)	15.192(015)	DAO	CTIO 0.9-m
511.56	...	17.857(017)	16.529(015)	16.136(011)	15.825(015)	...	DAO	YALO
511.57	...	17.892(018)	16.512(015)	16.140(011)	15.807(015)	...	DAO	YALO
513.59	...	17.956(031)	16.617(015)	16.257(011)	15.955(015)	...	DAO	YALO

Table 4—Continued

JD-2,451,000	<i>U</i>	<i>B</i>	<i>V</i>	<i>R</i>	<i>I</i>	<i>z</i>	Method	Telescope
513.60	...	18.005(031)	16.630(015)	16.250(011)	15.963(015)	...	DAO	YALO
515.59	...	18.026(030)	16.667(015)	16.317(011)	16.044(015)	...	DAO	YALO
515.60	...	18.012(022)	16.661(015)	16.307(011)	16.006(015)	...	DAO	YALO
517.53	...	18.002(019)	16.732(015)	16.395(011)	16.106(015)	...	DAO	YALO
517.54	18.906(181)	18.004(020)	16.737(015)	16.398(011)	16.128(015)	...	DAO	YALO
519.53	...	18.076(022)	16.774(015)	16.467(011)	16.212(015)	...	DAO	YALO
519.54	...	18.092(023)	16.775(015)	16.472(011)	16.206(015)	...	DAO	YALO
521.58	...	18.110(021)	16.833(015)	16.534(011)	16.287(015)	...	DAO	YALO
521.59	...	18.106(021)	16.832(015)	16.535(011)	16.266(015)	...	DAO	YALO

Note. — DAO means PSF photometry, while PHOT means aperture photometry

Table 5. Wavelength Shifts to Instrumental Bandpasses

Telescope	B (Å)	V (Å)	R (Å)	I (Å)	z (Å)
CTIO 0.9-m	0	15 blue	30 blue	90 red	50 blue
YALO	30 red	120 blue	180 blue	10 blue	...

Table 6. Lightcurve Parameters

Filter	Peak Mag.	JD Max
SN 1999ee		
<i>U</i>	14.74(0.06)	467.5(0.5)
<i>B</i>	14.93(0.02)	469.1(0.5)
<i>V</i>	14.61(0.03)	471.7(0.5)
<i>R</i>	14.53(0.02)	470.8(0.5)
<i>I</i>	14.66(0.02)	466.3(0.5)
<i>z</i>	14.50(0.05)	468.5(1.0)
SN 1999ex		
<i>U</i>	17.43(0.12)	496.2(0.5)
<i>B</i>	17.35(0.02)	498.1(0.5)
<i>V</i>	16.63(0.04)	501.2(0.5)
<i>R</i>	16.26(0.02)	502.7(0.5)
<i>I</i>	15.98(0.02)	502.6(0.5)
<i>z</i>	15.82(0.05)	504.2(1.0)

Table 7. *UBVRIz* Photometry for SN 1999ex

JD-2,451,000	<i>U</i>	<i>B</i>	<i>V</i>	<i>R</i>	<i>I</i>	<i>z</i>	Method	Telescope
481.55	19.876(108)	20.626(058)	20.414(057)	20.164(064)	19.816(101)	19.946(208)	DAO	CTIO 0.91-m
482.58	20.687(204)	20.689(109)	DAO	CTIO 0.91-m
482.61	20.500(163)	20.966(116)	20.157(079)	19.360(056)	19.592(147)	19.471(219)	DAO	CTIO 0.91-m
482.62	19.909(166)	19.489(080)	19.328(247)	0000000000	DAO	YALO
482.63	...	20.691(222)	20.141(198)	19.559(087)	19.316(314)	0000000000	DAO	YALO
483.65	19.609(039)	19.167(044)	18.990(051)	18.668(071)	DAO	CTIO 0.91-m
483.66	19.673(036)	DAO	CTIO 0.91-m
484.55	20.981(173)	20.339(055)	19.058(019)	18.608(023)	18.510(033)	18.165(034)	DAO	CTIO 0.91-m
484.58	...	20.183(119)	18.951(043)	18.569(023)	18.344(068)	...	DAO	YALO
484.58	...	20.183(119)	18.951(043)	18.569(023)	18.344(068)	...	DAO	YALO
484.59	...	20.058(107)	18.922(054)	18.533(027)	18.388(064)	...	DAO	YALO
484.59	...	20.058(107)	18.922(054)	18.533(027)	18.388(064)	...	DAO	YALO
485.60	20.040(132)	19.509(029)	18.461(019)	18.014(024)	17.969(034)	17.800(051)	DAO	CTIO 0.91-m
486.54	19.248(041)	18.920(017)	18.107(015)	17.715(017)	17.633(017)	17.417(025)	DAO	CTIO 0.91-m
486.62	...	18.928(044)	17.988(028)	17.676(015)	17.547(040)	...	DAO	YALO
486.62	...	18.928(044)	17.988(028)	17.676(015)	17.547(040)	...	DAO	YALO
486.63	...	18.858(042)	17.988(025)	17.666(015)	17.601(041)	...	DAO	YALO
486.63	...	18.858(042)	17.988(025)	17.666(015)	17.601(041)	...	DAO	YALO
487.53	18.788(033)	18.525(014)	17.791(015)	17.431(015)	17.354(019)	17.101(021)	DAO	CTIO 0.91-m
488.50	17.570(027)	DAO	D 1.54-m
488.53	17.613(020)	PHOT	D 1.54-m
488.58	18.422(029)	18.252(015)	17.547(017)	17.254(016)	17.161(015)	16.884(019)	DAO	CTIO 0.91-m
488.63	18.359(145)	18.236(024)	17.494(017)	17.200(011)	17.072(022)	...	DAO	YALO
488.64	18.307(150)	18.212(024)	17.476(015)	17.194(011)	17.004(018)	...	DAO	YALO
489.53	18.196(030)	18.021(014)	17.368(015)	17.077(017)	16.943(017)	16.707(018)	DAO	CTIO 0.91-m

Table 7—Continued

JD-2,451,000	<i>U</i>	<i>B</i>	<i>V</i>	<i>R</i>	<i>I</i>	<i>z</i>	Method	Telescope
490.53	17.975(022)	17.831(014)	17.217(015)	16.915(017)	16.801(016)	...	DAO	CTIO 0.91-m
490.63	17.762(094)	17.835(017)	17.141(015)	16.859(011)	16.735(017)	...	DAO	YALO
490.64	17.686(083)	17.811(017)	17.136(015)	16.863(011)	16.748(017)	...	DAO	YALO
492.52	17.679(018)	17.550(014)	16.968(015)	16.683(015)	16.514(015)	...	DAO	CTIO 0.91-m
492.62	17.426(069)	17.556(017)	16.931(015)	16.643(011)	16.490(015)	...	DAO	YALO
492.63	17.783(135)	17.565(017)	16.906(015)	16.642(011)	16.488(015)	...	DAO	YALO
493.54	17.563(017)	17.470(014)	16.900(015)	16.585(015)	16.427(015)	...	DAO	CTIO 0.91-m
495.57	17.460(017)	17.379(014)	16.777(015)	16.460(015)	16.278(016)	...	DAO	CTIO 0.91-m
495.59	17.304(057)	17.391(017)	16.720(015)	16.424(011)	16.233(015)	...	DAO	YALO
495.60	17.265(064)	17.395(017)	16.719(015)	16.412(011)	16.222(015)	...	DAO	YALO
496.56	17.503(017)	17.355(014)	16.740(015)	16.393(015)	16.185(015)	...	DAO	CTIO 0.91-m
496.66	...	17.326(013)	...	16.407(015)	PHOT	NTT
497.54	17.486(108)	17.340(019)	16.653(015)	16.329(011)	16.094(015)	...	DAO	YALO
497.55	17.371(058)	17.353(017)	16.665(015)	16.335(011)	16.116(015)	...	DAO	YALO
498.54	17.520(070)	17.364(017)	16.627(015)	16.298(011)	16.068(015)	...	DAO	YALO
498.54	17.537(017)	PHOT	CTIO 1.5-m
498.55	17.454(077)	17.351(019)	16.647(015)	16.310(011)	16.072(015)	...	DAO	YALO
498.56	17.559(022)	17.332(014)	16.668(015)	16.331(015)	16.097(015)	...	PHOT	CTIO 1.5-m
498.57	...	17.334(014)	16.670(015)	16.325(015)	16.103(015)	...	PHOT	CTIO 1.5-m
499.56	17.562(060)	17.363(017)	16.615(015)	16.285(011)	16.029(015)	...	DAO	YALO
499.57	17.528(079)	17.375(017)	16.629(015)	16.283(011)	16.015(015)	...	DAO	YALO
499.66	17.607(022)	17.376(014)	16.671(015)	16.299(015)	16.050(015)	...	DAO	CTIO 0.91-m
500.54	17.574(070)	17.408(017)	16.628(015)	16.263(011)	15.986(015)	...	DAO	YALO
500.55	17.614(085)	17.411(017)	16.608(015)	16.257(011)	15.983(015)	...	DAO	YALO
501.52	17.618(103)	17.450(017)	16.600(015)	16.247(011)	15.984(015)	...	DAO	YALO

Table 7—Continued

JD-2,451,000	<i>U</i>	<i>B</i>	<i>V</i>	<i>R</i>	<i>I</i>	<i>z</i>	Method	Telescope
501.53	17.720(090)	17.418(017)	16.619(015)	16.253(011)	15.967(015)	...	DAO	YALO
501.55	17.855(026)	DAO	CTIO 0.91-m
501.57	17.811(027)	17.474(014)	16.680(015)	16.285(015)	16.039(015)	15.823(015)	DAO	CTIO 0.91-m
503.52	17.981(159)	17.541(017)	16.660(015)	16.260(011)	15.966(015)	...	DAO	YALO
503.53	18.214(167)	17.563(017)	16.639(015)	16.267(011)	15.974(015)	...	DAO	YALO
504.53	...	17.623(021)	16.691(015)	16.279(011)	15.988(015)	...	DAO	YALO
504.54	...	17.620(020)	16.678(015)	16.270(011)	15.970(015)	...	DAO	YALO
505.52	...	17.717(020)	16.723(015)	16.316(011)	15.988(015)	...	DAO	YALO
505.53	18.352(155)	17.708(019)	16.716(015)	16.294(011)	15.994(015)	...	DAO	YALO
506.55	18.484(050)	17.815(014)	16.845(015)	16.343(015)	16.072(015)	15.855(017)	DAO	CTIO 0.91-m
507.58	...	17.932(024)	16.851(015)	16.398(011)	16.038(015)	...	DAO	YALO
507.59	...	17.930(024)	16.877(015)	16.390(011)	16.070(015)	...	DAO	YALO
508.54	...	18.066(018)	16.922(015)	16.448(011)	16.089(015)	...	DAO	YALO
508.55	...	18.060(018)	16.907(015)	16.433(011)	16.120(015)	...	DAO	YALO
508.58	18.966(041)	18.062(014)	16.972(015)	16.435(015)	16.130(015)	15.875(015)	DAO	CTIO 0.91-m
509.55	19.041(045)	18.154(014)	...	16.496(015)	16.173(015)	15.925(015)	DAO	CTIO 0.91-m
511.56	...	18.437(021)	17.203(015)	16.654(011)	16.232(015)	...	DAO	YALO
511.57	...	18.452(023)	17.196(015)	16.651(011)	16.244(015)	...	DAO	YALO
513.59	...	18.674(057)	17.421(025)	16.799(013)	16.337(020)	...	DAO	YALO
513.60	...	18.580(049)	17.371(023)	16.782(013)	16.337(021)	...	DAO	YALO
515.59	...	18.801(052)	17.514(021)	16.937(012)	16.484(021)	...	DAO	YALO
515.60	...	18.942(052)	17.489(020)	16.921(012)	16.452(016)	...	DAO	YALO
517.53	...	19.035(040)	17.663(018)	17.046(012)	16.573(016)	...	DAO	YALO
517.54	...	19.073(042)	17.688(017)	17.058(011)	16.568(017)	...	DAO	YALO
519.53	...	19.173(053)	17.803(020)	17.162(012)	16.629(020)	...	DAO	YALO

Table 7—Continued

JD-2,451,000	<i>U</i>	<i>B</i>	<i>V</i>	<i>R</i>	<i>I</i>	<i>z</i>	Method	Telescope
519.54	...	19.214(053)	17.774(016)	17.162(011)	16.639(017)	...	DAO	YALO
521.58	...	19.202(046)	17.894(024)	17.245(013)	16.684(020)	...	DAO	YALO
521.59	...	19.254(045)	17.875(029)	17.242(014)	16.770(020)	...	DAO	YALO

Note. — DAO means PSF photometry, while PHOT means aperture photometry

Table 8. Temperatures, Angular Radii, and Luminosities for SN 1999ex

$t - t_0$ (days)	T_{BVI} (K)	θ_{BVI} (10^{11} cm Mpc $^{-1}$)	$\log L(BB)$ (ergs s $^{-1}$)	$\log L(U \rightarrow z)$ (ergs s $^{-1}$)
1.04	12918(1415)	23(3)	41.440	41.021
2.06	9656(1199)	36(7)	41.332	41.063
2.09	7998(821)	48(9)	41.243	41.046
2.10	7373(1088)	60(17)	41.303	41.082
2.11	8210(1768)	49(18)	41.302	41.067
3.11	8721(547)	54(5)	41.503	41.196
3.12	8334(485)	57(5)	41.470	41.190
4.00	7747(233)	83(4)	41.664	41.363
4.03	7580(468)	91(10)	41.705	41.403
4.04	7900(486)	83(8)	41.704	41.419
5.04	7360(164)	117(5)	41.878	41.621
5.97	8656(126)	105(2)	42.060	41.790
6.05	8415(290)	116(7)	42.097	41.812
6.06	8945(329)	106(6)	42.126	41.818
6.95	9006(134)	114(3)	42.206	41.925
7.91	9705(144)	110(2)	42.304	42.013
7.94	9731(144)	111(2)	42.311	42.011
7.99	9794(146)	112(2)	42.329	42.021
8.04	9485(207)	122(4)	42.353	42.039
8.05	9425(183)	126(4)	42.365	42.049
8.93	9718(149)	125(3)	42.415	42.102
9.91	10115(157)	127(3)	42.498	42.169
10.01	9753(164)	137(3)	42.503	42.193
10.02	10011(173)	133(3)	42.518	42.198
11.88	10119(152)	144(3)	42.607	42.273
11.98	10061(164)	147(3)	42.614	42.291
11.99	10013(163)	148(3)	42.614	42.279
12.89	10067(150)	150(3)	42.635	42.307
14.90	9630(141)	169(4)	42.662	42.353
14.92	9441(143)	177(4)	42.667	42.369
14.93	9345(139)	180(4)	42.664	42.372
15.87	9225(124)	185(4)	42.663	42.369

Table 8—Continued

$t - t_0$ (days)	T_{BVI} (K)	θ_{BVI} ($10^{11} \text{cm Mpc}^{-1}$)	$\log L(BB)$ (ergs s^{-1})	$\log L(U \rightarrow z)$ (ergs s^{-1})
15.97	9320(122)	183(4)	42.673	42.373
16.84	8970(134)	199(5)	42.682	42.391
16.85	8953(127)	198(4)	42.673	42.391
17.83	8651(118)	212(5)	42.670	42.394
17.83	8651(118)	212(5)	42.670	42.394
17.84	8790(129)	206(5)	42.676	42.395
17.85	8853(113)	202(4)	42.671	42.388
17.86	8875(114)	201(4)	42.670	42.388
18.84	8453(112)	221(5)	42.669	42.398
18.85	8316(108)	227(5)	42.662	42.397
18.94	8382(100)	221(4)	42.652	42.387
19.81	8035(100)	240(5)	42.652	42.397
19.82	8022(100)	242(5)	42.654	42.398
20.78	7877(96)	248(5)	42.646	42.396
20.79	7912(97)	247(5)	42.650	42.395
20.81	7900(92)	244(5)	42.636	42.382
20.83	7888(88)	241(5)	42.621	42.374
22.75	7432(85)	270(6)	42.616	42.371
22.76	7401(84)	271(6)	42.615	42.365
23.75	7366(92)	270(6)	42.602	42.350
23.76	7281(87)	277(6)	42.604	42.353
24.73	7026(81)	289(6)	42.579	42.332
24.74	7045(79)	288(6)	42.579	42.335
25.75	6776(63)	293(6)	42.528	42.299
26.77	6656(78)	305(7)	42.531	42.280
26.78	6739(80)	294(7)	42.523	42.276
27.72	6261(60)	329(7)	42.491	42.249
27.73	6373(63)	316(6)	42.488	42.251
27.76	6246(53)	323(6)	42.473	42.242
28.72	6121(51)	327(6)	42.447	42.215
30.70	5794(55)	346(7)	42.402	42.139
30.71	5859(59)	338(7)	42.401	42.138

Table 8—Continued

$t - t_0$ (days)	T_{BVI} (K)	θ_{BVI} (10^{11} cm Mpc $^{-1}$)	$\log L(BB)$ (ergs s $^{-1}$)	$\log L(U \rightarrow z)$ (ergs s $^{-1}$)
32.71	5750(100)	328(12)	42.341	42.061
32.72	5902(100)	316(11)	42.353	42.075
34.69	5889(100)	297(10)	42.296	42.005
34.70	5787(84)	309(9)	42.301	42.003
36.60	5580(70)	312(8)	42.244	41.945
36.61	5517(70)	319(9)	42.244	41.939
38.58	5413(81)	319(11)	42.212	41.897
38.59	5574(75)	302(9)	42.216	41.897
40.61	5272(76)	325(11)	42.182	41.867
40.62	5381(82)	302(10)	42.154	41.858

Note. — Adopted values: $E(B - V)_{Gal}=0.02$, $E(B - V)_{host}=0.28$,
 $D=51.16$ Mpc, $t_0=$ JD 2,451,480.5